EurJIC
European Journal of Inorganic Chemistry

Review
doi.org/10.1002/ejic.202400220

Chemistry Europe
European Chemical Societies Publishing

www.eurjic.org

Isomerism in Molecular Metal Carbonyl Clusters

Cristiana Cesari,[a] Cristina Femoni,[a] Francesca Forti,[a] Maria Carmela Iapalucci,[a] Giorgia Scorzoni,[a] and Stefano Zacchini*[a]

The present microreview focuses on different typologies of isomerism documented along the years for metal carbonyl clusters (MCCs), and outlines their analogies to other classes of ligand-protected molecular clusters and nanoclusters. Isomerism in molecular MCCs is discussed within two main categories, that is, surface isomerism and core isomerism. The first Section presents some representative examples of surface isomerism involving inorganic (carbonyls and hydrides) and organic ligands, as well as isomerism due to ML fragments decorating the cluster surface. The second Section focuses on three major categories of core isomerism, that is: (1) isomers that mainly differ on M–M distances; (2) isomers displaying different structures of the metal kernels; (3) isomers possessing almost identical metal kernels and ligand shells, but differing for the positions of different types of metal atoms within the metal kernel. The third Section briefly discusses two related and very rare cases of isomerism, that is, polymerisation and coordination isomerism. General conclusions are outlined in the final Section.

Introduction

Isomerism is a key topic in organic and coordination chemistry, widely discussed in most undergraduate textbooks. Isomeric compounds may be broadly classified into two major categories, that is, stereoisomers and structural isomers. More recently, isomerism has been investigated also in the field of molecular metal clusters and atomically precise metal nanoclusters, in view of their relevance to nanochemistry and nanotechnologies.[1–9] Most of these studies have been dedicated to Au nanoclusters, and related coinage metal ligand protected molecular nanoclusters. Examples of isomerism in such nanoclusters include enantiomerism, and different types of structural isomerism, that is, core isomerism, staple isomerism and complex isomerism. Ligand protected metal nanoclusters are composed of a metal core and a ligand shell. Thus, isomerism may involve the stereochemistry of the ligands, their position and/or coordination mode, the staple motives on the surface of the cluster, the structure of the metal core, the disposition of different metal types within the metal kernel, or a combination of these.[10–17]

Even though isomerism is possible and has been documented for other classes of molecular metal clusters, systematic studies are very rare or completely missing.[18,19] Probably the first example of cluster core isomerism is represented by the organometallic cluster $[Pt_3(\mu\text{-}PPh_2)_3Ph(PPh_3)_2]$, whose two isomers have been described for the first time in 1985.[20–22] Since then, other examples of isomerism in organometallic clusters and, in particular, metal carbonyl clusters (MCCs) have been reported (Scheme 1). It must be remarked that the study of MCCs of increasing sizes may contribute to a better understanding of atomically precise metal nanoparticles, metal nanoclusters, ultra-small metal nanoparticles and nanomaterials in general.[23–30] Moreover, MCCs have found applications in catalysis and electrocatalysis.[31–34] In this perspective, a rationalization of isomerism in molecular MCCs could help deepening our insights into isomerism at nanometric and sub-nanometric sizes.

Within this framework, we report herein a microreview on isomerism in MCCs. This is not intended to be a systematic and comprehensive review. Instead, general principles will be discussed and supported by some representative examples, particularly focusing on our own recent contribution to the field. The first Section deals with surface isomerism in MCCs. This may involve inorganic (mainly CO and hydride) or organic ligands, as well as ML fragments decorating the surface of the cluster. The following Section focuses on core isomerism, and it is broadly divided into three sub-sections: (1) isomers that mainly differ on M–M distances; (2) isomers displaying different structures of the metal kernels; (3) heterometallic MCCs possessing almost identical metal kernels and ligand shells, but differing for the positions of different types of metal atoms within the metal kernel. The third Section briefly discusses two related and very rare cases of isomerism, that is, polymerisation and coordination isomerism.

It must be remarked that, in some cases, different types of isomerism occur at the same time and, thus, their classification within a single category is not straightforward. Where possible, the different types of isomerism will be discussed considering MCCs of different sizes, in order to show how these concepts apply across different size regimes. All the examples reported in this microreview are based on isomeric MCCs structurally characterized by single crystal X-ray diffraction (SC-XRD), in some cases further supported by spectroscopic studies in solution. Details of their syntheses may be found in the cited literature. In some cases, different isomers have been selectively obtained following different synthetic procedures, whereas other isomeric MCCs have been obtained as mixtures, that can

[a] C. Cesari, C. Femoni, F. Forti, M. C. Iapalucci, G. Scorzoni, S. Zacchini
Dipartimento di Chimica Industriale "Toso Montanari", Università di Bologna, Via Piero Gobetti 85, 40129 Bologna, Italy
E-mail: stefano.zacchini@unibo.it

or cannot be separated. Dynamic equilibria in solution between isomers have been also sometimes detected.

IUPAC definition of isomer has been used all along this microreview: "One of several species (or molecular entities) that have the same atomic composition (molecular formula) but different line formulae or different stereochemical formulae and hence different physical and/or chemical properties."[35] In order to help the reader, the sum formula of the isomers and the type of isomerism is reported in each Figure. The following discussion will be mainly focused on examples where all isomers have been isolated and structurally characterized.

Cristiana Cesari received the Master Degree in Industrial Chemistry from the University of Bologna in 2012, and in 2016 was awarded a Ph.D. in Chemistry from the University of Bologna. Her doctoral research was focused on the synthesis, characterization and catalytic application of ruthenium N-heterocyclic carbene complexes. After a post-doctoral fellowship in Bologna focused on the study of the transformation process of ethanol to butanol via both homogeneous and heterogeneous catalysis, in 2019, she became a researcher in the field of General and Inorganic Chemistry at the University of Bologna. Her research activityis aimed at the synthesis of molecular organometallic compounds containing low valent transition metals stabilized by ligands, focusing on the study of metal carbonyl cluster as atomically defined nanomaterials for electrochemical applications and as precursors of nanostructured catalytic systems.

Cristina Femoni received her Degree cum laude in Industrial Chemistry from the University of Bologna working on an experimental thesis under the supervision of Prof. G. Longoni. After a brief industrial working experience in France, in 1999 she was awarded a PhD in Chemical Sciences from the University of Bologna. Since 2022 she is full professor of General and Inorganic Chemistry. Her main scientific interests and expertise lie in the synthesis and characterization, also by single-crystal X-ray diffraction, of high-nuclearity transition metal clusters stabilized by carbonyl ligands, also referred to as atomically-precise ligand-stabilized nanoclusters, and their application in catalysis and nanoscience. She has been elected President of the European Chemistry Thematic Network (ECTN).

Francesca Forti received the Master Degree in Industrial Chemistry from the University of Bologna in 2021, and the same year started her Ph.D. in Chemistry at the University of Bologna. Her doctoral research is focused on the synthesis and characterization of new heterometallic carbonyl clusters and their application in catalytic reactions. In 2023 she joined Professor Nordlander's group in University of Lund for a visiting period to conduct synthesis and characterization of Os-Rh carbonyl clusters bearing chiral phosphines, exploited as asymmetric catalysts.

Maria Carmela Iapalucci received the Degree in Industrial Chemistry from the University of Bologna in 1987 with an experimental thesis under the supervision of Prof. G. Rosini. In 1992, she received her PhD in Chemical Sciences from the University of Bologna, working on the synthesis and characterization of iron and nickel carbonyl clusters containing group XIII and XV heteroatoms, under the supervision of Prof. G. Longoni. Since 2001 she is associate professor of General and Inorganic Chemistry at the University of Bologna.

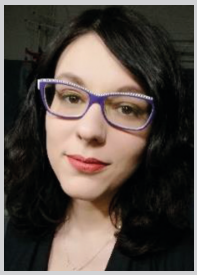

Giorgia Scorzoni received the Master Degree in Industrial Chemistry from the University of Bologna in 2022. After spending one year as a research fellow in the field of Inorganic Chemistry, she started her Ph.D. in Industrial Chemistry at the University of Bologna. Her research activities focus on synthesis and characterization of new rhodium carbonyl clusters differentially substituted.

Stefano Zacchini received the Degree in Industrial Chemistry from the University of Bologna in 1996, working on an experimental Thesis under the supervision of Prof G. Longoni. In 2001, he received his PhD in Chemistry from the University of Liverpool under the direction of Prof B. T. Heaton. After a post-doctoral fellowship in Liverpool, he joined the University of Bologna in 2002 as research associate. In 2010, he has been appointed Associate Professor of General and Inorganic Chemistry at the University of Bologna and in 2017 he became full Professor. His research program focuses on the chemistry of metal carbonyl clusters and their applications in nanotechonolgy and nanosciences, molecular electronics and catalysis.

Review
doi.org/10.1002/ejic.202400220

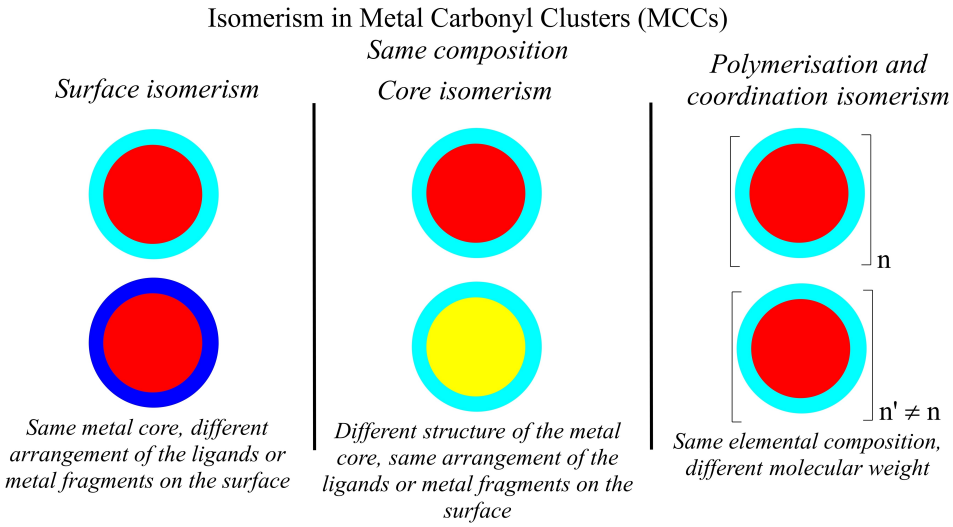

Scheme 1. Isomerism in Metal Carbonyl Clusters (MCCs). Two MCC isomers have the same composition, but they have a different arrangement of the ligands or metal fragments on the surface (surface isomerism), or a different structure of the metal core (core isomerism), or different molecular weights (polymerization and coordination isomerism).

Surface Isomerism

Surface Isomerism Involving Inorganic and Organic Ligands

The most straightforward source of isomerism in MCCs is represented by CO ligands, that can bind to the metal core in miscellaneous fashions.[23,36] These include terminal, edge bridging and face capping coordination, with different levels of asymmetry as well as other less common coordination modes. Often MCCs are fluxional in solution, indicating rapid exchange of the CO ligands. In some cases, isomers showing a different stereochemistry of the carbonyls have been isolated and structurally characterized in the solid state.

$[Co_2(CO)_8]$ adopts in the solid state a C_{2v} $[Co_2(\mu\text{-}CO)_2(CO)_6]$ structure, but unbridged D_{3d} and D_{2d} isomers have been also spectroscopically detected in solution (Scheme 2).[37] Eventually, the D_{3d} isomer has been trapped and structurally characterized by SC-XRD as the $[Co_2(CO)_8]{\cdot}C_{60}$ adduct.

Isomers showing a different stereochemistry of the CO ligands have been structurally characterized also in the case of $[Rh_3Cp_3(CO)_3]$,[38] $[Ir_6(CO)_{16}]$,[39] $[Fe_4Au(CO)_{16}]^-$(Figure 1),[40,41] $[Ru_3Ir(CO)_{13}]^-$,[42] $[HRu_3Ir_2(CO)_{14}]^-$,[43] and $[Co_4(CO)_{11}]^{2-}$.[44]

Isomerism due to CO ligands may arise not only from their coordination mode, but also from their disposition (stereochemistry) around the metal core. Just to exemplify this concept, three isomers of the heterometallic cluster $[Cu\{Co(CO)_4\}_2]^-$ have been characterized by SC-XRD. All of them contain only terminal carbonyls, but they differ for the overall arrangement of the CO ligads around Co-atoms, that is, TBP-TBP eclipsed, TBP-TBP staggered, and TBP–Td (TPB = trigonal

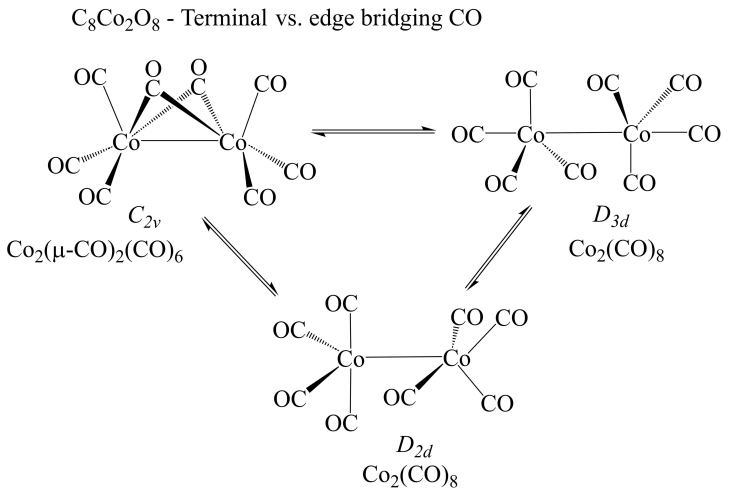

Scheme 2. Surface isomerism – Different coordination mode of the CO ligands. Solution equilibria involving the bridged C_{2v} $[Co_2(\mu\text{-}CO)_2(CO)_6]$, and unbridged D_{3d} and D_{2d} $[Co_2(CO)_8]$ isomers. The three isomers have been spectroscopically (by IR) detected in solution. The bridged C_{2v} $[Co_2(\mu\text{-}CO)_2(CO)_6]$ isomer is the one usually present within crystals. The unbridged D_{3d} isomer has been trapped and structurally characterized by SC-XRD as the $[Co_2(CO)_8]{\cdot}C_{60}$ adduct.

Review
doi.org/10.1002/ejic.202400220

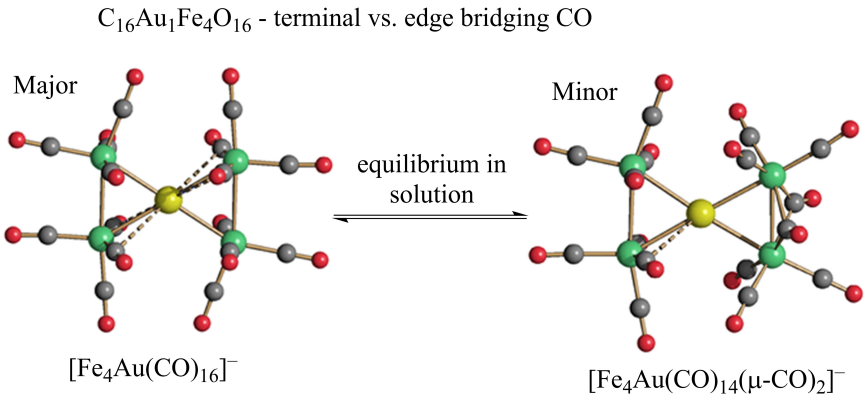

Figure 1. Surface isomerism – Different coordination mode of the CO ligands. Molecular structures of the $[Fe_4Au(CO)_{16}]^-$ (all terminal) and $[Fe_4Au(CO)_{14}(\mu\text{-}CO)_2]^-$ (bridging) isomers. Sub Van der Waals Au···C(O) contacts are represented as fragmented lines (yellow, Au; green, Fe; red, O; grey, C). The two isomers are in equilibrium in solution, being the all terminal isomer $[Fe_4Au(CO)_{16}]^-$ the major species.[41] The isomer found in the solid state depends upon crystallization conditions. The all terminal isomer has been isolated as $[NMe_3(CH_2Ph]_2[Fe_4Au(CO)_{16}]Cl$, whereas the bridging isomer has been crystallized as $[NEt_4][Fe_4Au(CO)_{14}(\mu\text{-}CO)_2]$ and $[EtV][Fe_4Au(CO)_{14}(\mu\text{-}CO)_2]\cdot 2THF$ (EtV = ethylviologen = 1,1′-Diethyl-4,4′-bipyridinium).

bipyramid; Td = tetrahedron).[45] All the three isomers contain a linear Co–Cu-Co core, with four terminal CO ligands per Co-atom (Figure 2). In the TBP-TBP eclipsed and TBP-TBP staggered isomers, both Co-centres adopt a trigonal bipyramidal coordination, with three carbonyls in the equatorial plane, whereas the fourth CO and Cu occupy the apical positions. The TBP-TBP eclipsed and TBP-TBP staggered isomers differ because the two TBP $Co(CO)_4$ groups adopt an eclipsed conformation in the former, and a staggered conformation in the latter. The same two isomers have been isolated for the neutral $Hg[Co(CO)_4]_2$ cluster.[46] In the third isomer of $[Cu\{Co(CO)_4\}_2]^-$ (TBP–Td), one Co centre is TPB and the second one displays a tetrahedral coordination, with Cu capping one edge of the $Co(CO)_4$ tetrahedron. In all isomers, sub van der Waals Cu···C(O) contacts are present, three per each TBP–$Co(CO)_4$ group, and two for Td–$Co(CO)_4$.

Isomerism due to the different stereochemistry of the CO ligands is not limited to lower nuclearity MMCs, and is somehow related to carbonyl fluxionality detected in solution by variable temperature NMR spectroscopy. Nonetheless, only in very few cases such isomers differing for the CO binding mode have been isolated and structurally characterized in the case of larger MCCs. For instance, in the case of $[Rh_{12}Sn(CO)_{27}]^{2-}$, two isomers are present within the unit cell of the same crystal, one displaying 13 terminal and 14 edge-bridging CO ligands, whereas the second isomer possesses 12 terminal and 15 edge-bridging carbonyls (Figure 3).[47] For these two isomers, also some Rh–Rh and Rh–Sn contacts are sensibly different, even though the average values are very similar. ^{13}C-{^{103}Rh} HMQC NMR studies show a single broad resonance at 273 K for the CO ligands ($\delta_C = 220.5$ ppm) and the Rh atoms ($\delta_{Rh} = -610$ ppm), indicating rapid scrambling of the carbonyls around the metal icosahedron. Coalescence of the CO resonances occurs at 213 K, and two almost equally intense broad resonances appear at 183 K, attributable to terminal ($\delta_C = 206$ ppm) and bridging ($\delta_C = 236$ ppm) carbonyls. A similar isomerism due to a different

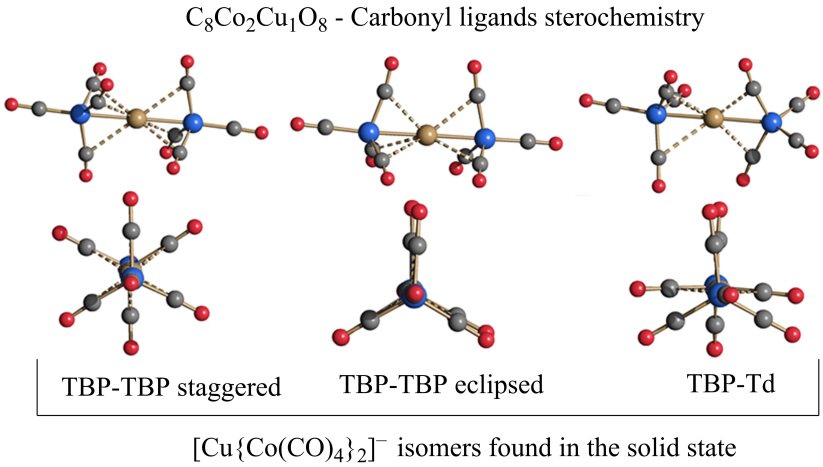

Figure 2. Surface isomerism – Different stereochemistry of the CO ligands. Two views of the three isomers of $[Cu\{Co(CO)_4\}_2]^-$. Sub Van der Waals Cu···C(O) contacts are represented as fragmented lines (brown, Cu; blue, Co; red, O; grey, C). Isomer TBP-TBP staggered has been determined as $[NEt_4][Cu\{Co(CO)_4\}_2]$ salt, TBP-TBP eclipsed as $[Cu(dmpe)_2][Cu\{Co(CO)_4\}_2]$ salt, TBP–Td as $[PPN][Cu\{Co(CO)_4\}_2]$ salt (dmpe = $Me_2PCH_2CH_2PMe_2$; $[PPN]^+ = [N(PPh_3)_2]^+$; TBP = trigonal bipyramid; Td=Tetrahedron).[45]

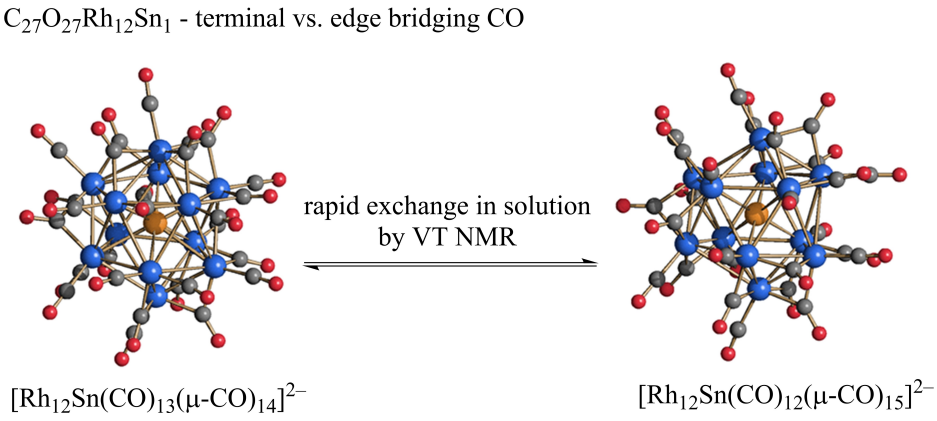

Figure 3. Surface isomerism – Different coordination mode of the CO ligands. Molecular structures of the $[Rh_{12}Sn(CO)_{13}(\mu\text{-}CO)_{14}]^{2-}$ (left) and $[Rh_{12}Sn(CO)_{12}(\mu\text{-}CO)_{15}]^{2-}$ (right) isomers of $[Rh_{12}Sn(CO)_{27}]^{2-}$ (blue, Rh; orange, Sn; red, O; grey, C). The two isomers are present in the same unit cell in a 1:1 ratio, and rapidly exchange in solution.[47]

stereochemistry of the CO ligands accompanied by some slight variations of the Rh–Rh contacts has been documented for $[Rh_{11}(CO)_{23}]^{-}$.[48]

A further source of isomerism is introduced in MCCs by hydride ligands, which can be found in terminal, edge bridging and face capping positions as in the case of CO ligands. In addition to the coordination mode, isomerism may arise also because of the different location of the hydrides around the metal cage of the cluster, sometimes also referred to the CO stereochemistry. Hydride MCCs are often fluxional in solution, and in several cases different isomers have been detected by VT ^{1}H NMR spectroscopy. The structural characterization of such isomers by SC-XRD is rather rare, and $[H_3Ru_4(CO)_{12}]^{-}$ represents the most significant example.[49–51] Two isomers, with C_2 and C_{3v} symmetry respectively, have been isolated, both displaying 12 terminal CO ligands (three per each Ru atom) and three μ-H ligands (Figure 4). The C_2 and C_{3v} isomers differ solely because of the different location of the three μ-H ligands around the Ru_4 tetrahedron.

Admitting organic ligands within the coordination sphere of MCCs introduces an additional potential source of isomerism. This can be due to the stereochemistry of the organic ligands, including coordination mode, orientation and/or position, as well as their structures. Several examples have been reported, involving different types of ligands. Only a few examples will be discussed herein, and the reader can find further examples in the literature.[52–54]

Among the different organic ligands employed in MCC chemistry, phosphines are probably the most common ones. Indeed, a large number of phosphine substituted MCCs is known.[23,24,27–29] Phosphine migration along a cluster core has been often observed in solution, and this may be somehow related to the fact that phosphine ligands may bind to the cluster core in different positions. As a consequence, isomers may arise due to phosphine coordination to different sites of a MCC.

For example, two isomers have been structurally characterized for $[WRu_3(\mu_4\text{-}Se)_2(CO)_{11}(tpnp)]$ (tpnp = trispyrrolidinylphosphine) (Figure 5).[55] In one isomer, tpnp is coordinated to Ru bonded to W, whereas in the second isomer tpnp is bonded to Ru opposite to W. The two isomers may be separated and display a slightly different electrochemical behaviour. Similarly, two isomers have been reported for $[HOs_3(CO)_8(OH)(PPh_3)_2]$, that differ in the substitution positions of PPh_3.[56]

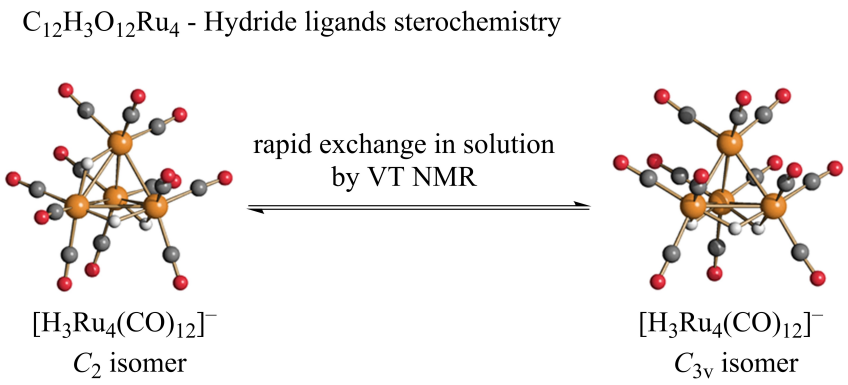

Figure 4. Surface isomerism – Different stereochemistry of the hydride ligands. Molecular structures of the C_2 and C_{3v} isomers of $[H_3Ru_4(CO)_{12}]^{-}$ (orange Ru; red O; grey C; white H). Both isomers are present in solution as shown by VT NMR experiments. Depending on the experimental conditions, the two isomers can be crystallized as separate compounds, or co-crystallized together.[49–51] Adapted from Ref.[51] with permission from The Royal Society of Chemistry.

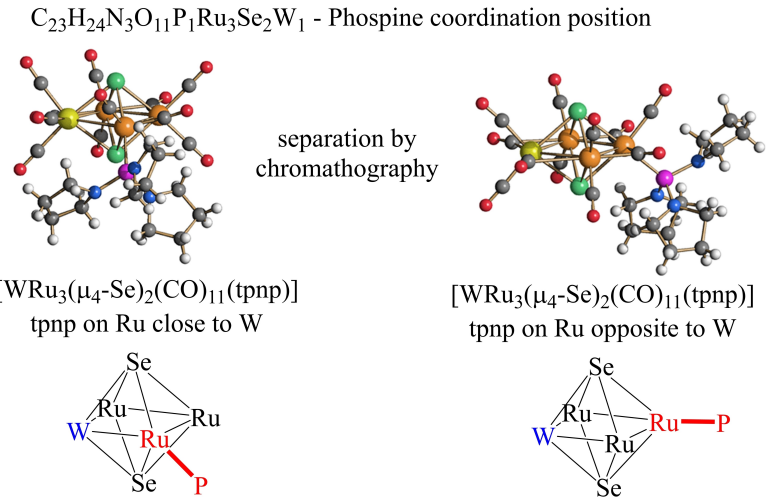

Figure 5. Surface isomerism – Different coordination sites of phosphine ligands. Molecular structures of the two isomers of $[WRu_3(\mu_4\text{-}Se)_2(CO)_{11}(tpnp)]$ (tpnp = trispyrrolidinylphosphine) differing for the location of the tpn ligand (orange Ru; yellow, W; green, Se; purple, P; red O; grey C; white H).[55]

Two isomers may contain the phosphine ligands bonded to the same sites, but with a different orientation. For instance, in the case of the Chini-type heteroleptic cluster $[Pt_9(CO)_{16}(R\text{-dppp})]^{2-}$ (*R*-dppp = *R*-$Ph_2PCH(Me)CH_2PPh_2$), the chiral *R*-dppp ligand bridges one outer and the inner triangular units, and two isomers are present both in solution and in the solid state due to the different orientation of *R*-dppp (Figure 6), as shown by $^{31}P\{^1H\}$ NMR spectroscopy and SC-XRD.[57]

In addition, bidentate phosphines may act as bridging or chelating ligands, and this may generate isomers, as found in

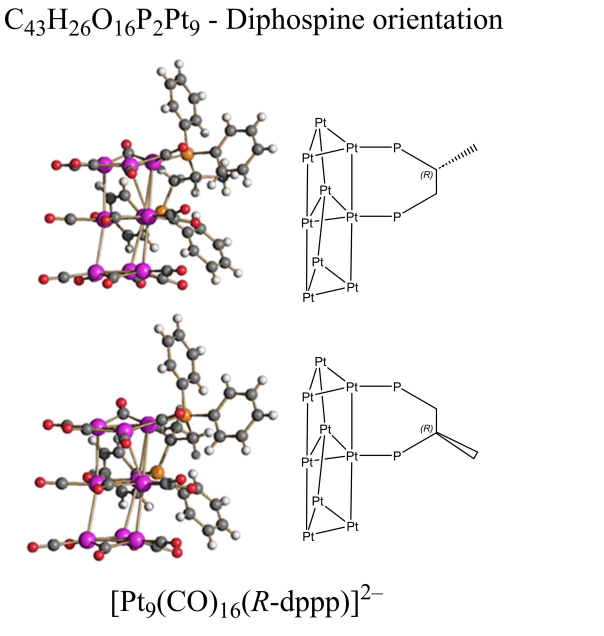

Figure 6. Surface isomerism – Different orientation of an asymmetric diphosphine ligand. Molecular structure of the two isomers of $[Pt_9(CO)_{16}(R\text{-dppp})]^{2-}$ (Pt, purple; P, orange; O, red; C, grey; H, white). The two isomers are present in a 1:1 ratio in the solid state structure. Adapted with permission from Ref.[57] Copyright 2017 American Chemical Society.

$[Fe_3Pt(\mu_4\text{-}Se)(CO)_9(dppm)]$ (dppm = $Ph_2PCH_2PPh_2$): in one isomer, dppm is chelating on Pt, whereas in the second isomer dppm bridges Pt and Fe (Figure 7).[58] These isomers may be separated by chromatography, but attain equilibrium in solution after one month as monitored by $^{31}P\{^1H\}$ NMR.

Surface isomerism in MCCs may be generated by several other classes of ligands and, indeed, numerous examples are known. A systematic discussion on this topic is outside the scope of the present microreview, and only a few representative cases will be herein presented.

The reaction of $[Os_3(CO)_{10}(MeCN)_2]$ with *closo*-*o*-$C_2B_{10}H_{10}$ yields two interconvertible isomers $[Os_3(CO)_9(\mu_3\text{-}4,5,9\text{-}C_2B_{10}H_8)(\mu\text{-}H)_2]$ and $[Os_3(CO)_9(\mu_3\text{-}3,4,8\text{-}C_2B_{10}H_8)(\mu\text{-}H)_2]$, where the carborane utilizes different atoms to bind the Os cluster (Figure 8).[59]

Aromatic and unsaturated compounds can bind to MCCs in several different fashions, and isomers have been often documented.[60,61] Some representative examples are the couples of isomers $[Ru_5C(CO)_{12}(\eta^6\text{-}C_6H_6)]$ and $[Ru_5C(CO)_{12}(\mu_3\text{-}\eta^2\text{-}\eta^2\text{-}\eta^2\text{-}C_6H_6)]$,[62] $[Os_3(CO)_{10}(\mu\text{-}\eta^1\text{-}2\text{-}Np)(\mu\text{-}AuPPh_3)]$ and $[Os_3(CO)_{10}(\mu\text{-}\eta^2\text{-}2\text{-}Np)(\mu\text{-}AuPPh_3)]$ (Np = 2-naphthyl, 2-$C_{10}H_7$),[63] $[Os_3(CO)_{10}(\mu\text{-}\eta^1\text{-}2\text{-}Pyryl)(\mu\text{-}AuPPh_3)]$ and $[Os_3(CO)_{10}(\mu\text{-}\eta^1\text{-}4\text{-}Pyryl)(\mu\text{-}AuPPh_3)]$ (Pyryl = $C_{16}H_9$),[63] $[Os_3(CO)_{10}(\mu_3\text{-}\eta^2\text{-}1,2\text{-}Pyryne)(\mu\text{-}AuPPh_3)(\mu\text{-}H)]$ and $[Os_3(CO)_{10}(\mu_3\text{-}\eta^2\text{-}4,5\text{-}Pyryne)(\mu\text{-}AuPPh_3)(\mu\text{-}H)]$ (Pyryne = $C_{16}H_8$),[63] $[Ru_6(\mu_6\text{-}C)(CO)_{14}[\eta^6\text{-}1,2\text{-}C_6H_4(CO_2Me)_2]$ and $[Ru_6(\mu_6\text{-}C)(CO)_{14}[\mu_3\text{-}\eta^6\text{-}1,2\text{-}C_6H_4(CO_2Me)_2]$ (Figure 9),[64] $[Os_3(\mu\text{-}H)_2(\mu_3\text{-}1\text{-}OC_{10}H_6)(CO)_9]$ and $[Os_3(\mu\text{-}H)_2(\mu\text{-}1\text{-}OC_{10}H_6)(CO)_9]$.[65] In all of these cases, the isomers differ because of the coordination mode of the aromatic ligand (e.g., η, μ, μ_3, $\mu\text{-}\eta^1$, $\mu\text{-}\eta^2$, η^6, $\mu_3\text{-}\eta^6$) and/or the C atoms used for coordination.

Three isomers have been isolated for $[Os_3(CO)_9(PPh_3)\{\mu\text{-}\eta^1,\kappa^1\text{-}C_9H_5N(6\text{-}OMe)\}(\mu\text{-}H)]$, which can be thermally interconverted.[66] These three isomers differ in the location of the metal-bound hydride and PPh_3 with respect to 6-methoxyquinolinate moiety. In the case of $[Mo_2Ir_2(\mu\text{-}CO)_3(AsPh_3)(CO)_6(\eta^5\text{-}C_5H_5)_2]$, two co-crystallized isomers differing for the disposition of the Cp group with respect to the arsine-

Review
doi.org/10.1002/ejic.202400220

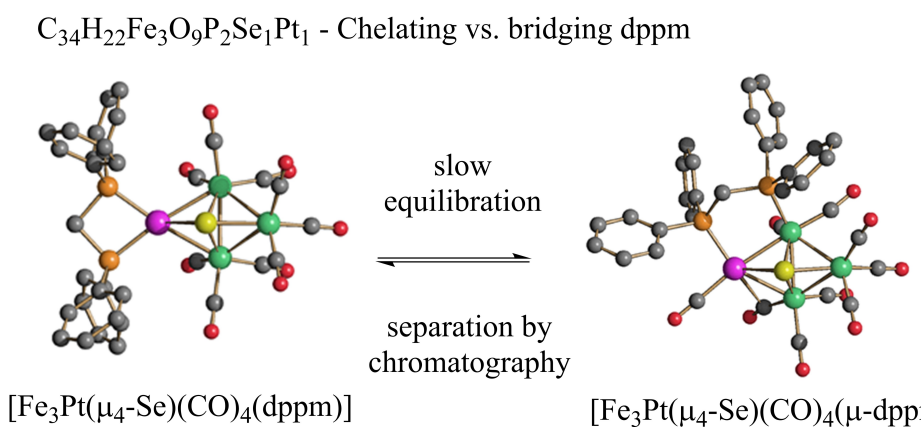

Figure 7. Surface isomerism – Different coordination modes of a bidentate phosphine ligand. Molecular structures of the two isomers of $[Fe_3Pt(\mu_4\text{-}Se)(CO)_9(dppm)]$ (dppm = $Ph_2PCH_2PPh_2$) that differ for the coordination mode of the dppm ligand: (left) dppm as chelating ligand and (right) dppm as bridging ligand (green, Fe; purple, Pt; yellow, Se; orange, P; red, O; grey, C). Hydrogen atoms have been omitted for clarity. The different coordination mode of dppm causes also some variations of the CO stereochemistry. The two isomer may be separated by chromatography, but attain equilibrium in solution after one month as monitored by $^{31}P\{^1H\}$ NMR.[58]

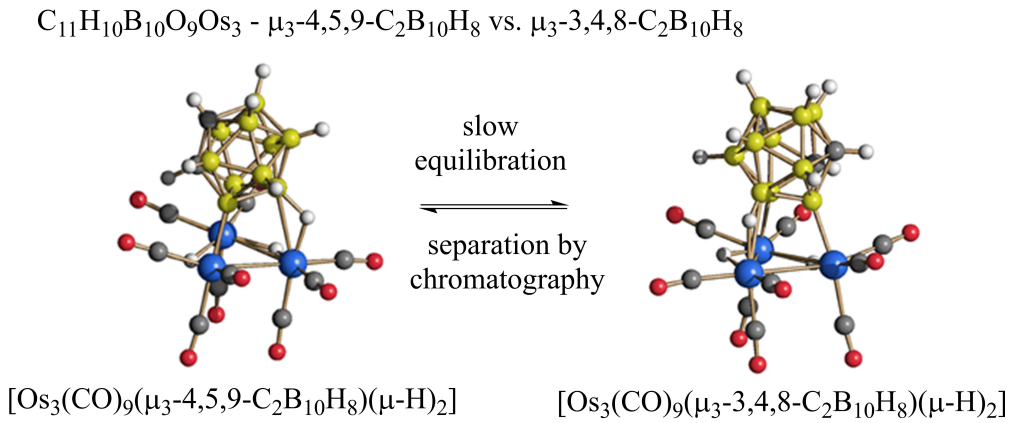

Figure 8. Surface isomerism – Different coordination modes of a carborane ligand. Molecular structures of the two isomers $[Os_3(CO)_9(\mu_3\text{–}4,5,9\text{-}C_2B_{10}H_8)(\mu\text{-}H)_2]$ and $[Os_3(CO)_9(\mu_3\text{-}3,4,8\text{-}C_2B_{10}H_8)(\mu\text{-}H)_2]$ that differ for the atoms used by the carborane to bind the cluster (blue, Os; yellow, B; red, O; grey, C; white, H). These two interconvertible isomers have been obtained from the reaction of $[Os_3(CO)_{10}(MeCN)_2]$ with *closo*-$C_2B_{10}H_{10}$.[59] Adapted from ref.[31] with permission from The Royal Society of Chemistry.

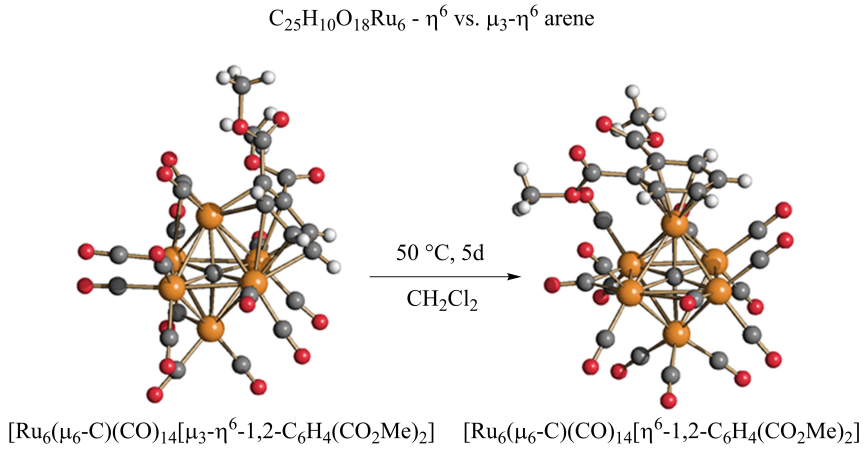

Figure 9. Surface isomerism – Different coordination modes of an arene ligand. Molecular structures of the two isomeric compounds $[Ru_6(\mu_6\text{-}C)(CO)_{14}[\eta^6\text{-}1,2\text{-}C_6H_4(CO_2Me)_2]$ and $[Ru_6(\mu_6\text{-}C)(CO)_{14}[\mu_3\text{-}\eta^6\text{-}1,2\text{-}C_6H_4(CO_2Me)_2]$, differing for the coordination mode of the 1,2-$C_6H_4(CO_2Me)_2$ ligand (orange Ru; red O; grey C; white H).[64] The two isomers may be viewed as snapshots of the arene ligand moving from a single Ru atom to a Ru_3 face of the octahedron.

Review
doi.org/10.1002/ejic.202400220

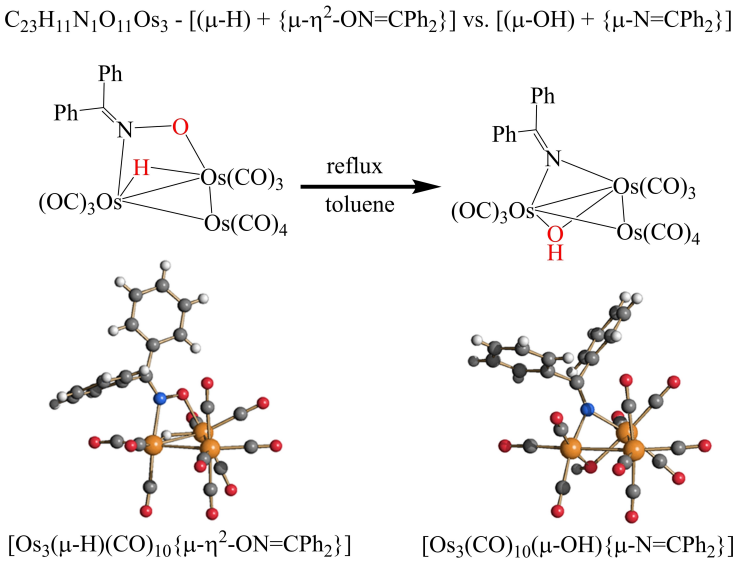

Figure 10. Surface isomerism – Different structures of the organic ligands. Molecular structures of the two isomeric compounds $[Os_3(\mu\text{-}H)(CO)_{10}\{\mu\text{-}\eta^2\text{-}ON{=}CPh_2\}]$ and $[Os_3(CO)_{10}(\mu\text{-}OH)\{\mu\text{-}N{=}CPh_2\}]$, having sum formula $Os_3C_{23}H_{11}NO_{11}$ (orange Os; blue, N; red O; grey C; white H). After thermal treatment, the edge bridging H and $ON{=}CPh_2$ ligands are transformed into OH and $N{=}CPh_2$.[71]

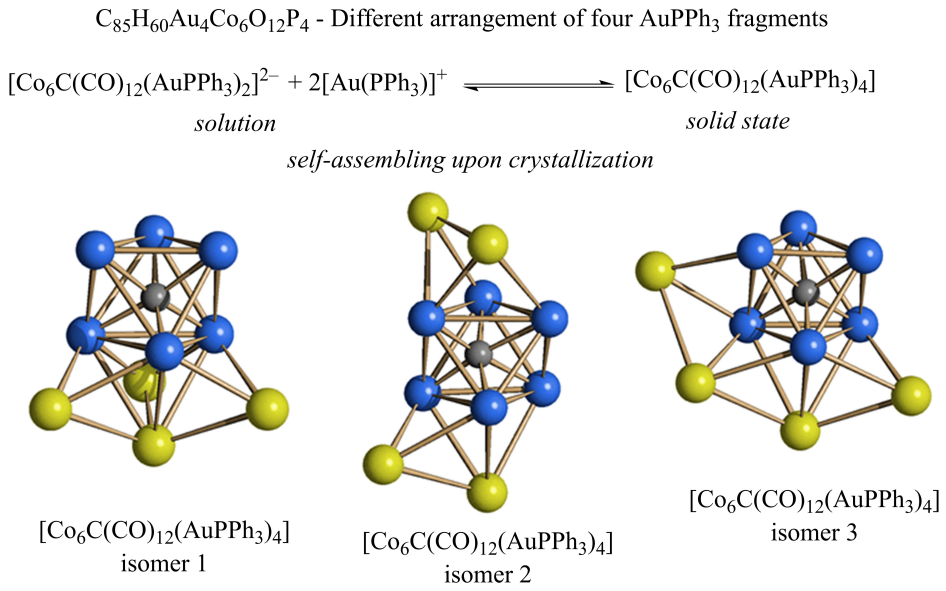

Figure 11. Surface isomerism – Different arrangement of $AuPPh_3$ fragments. The neutral cluster $[Co_6C(CO)_{12}(AuPPh_3)_4]$ self-assembles upon crystallisation of a solution containing $[Co_6C(CO)_{12}(AuPPh_3)_2]^{2-}$ and $Au(PPh_3)Cl$. Three different isomers may be found in the solid state, depending on the amount of co-crystallized solvent, that is, $[Co_6C(CO)_{12}(AuPPh_3)_4]$ (solvent-free) (isomer 1), $[Co_6C(CO)_{12}(AuPPh_3)_4]$·THF (isomer 2), and $[Co_6C(CO)_{12}(AuPPh_3)_4]$·4THF (isomer 3). The three isomers differ for the dispositions of the four $[Au(PPh_3)]^+$ fragments on the surface of the octahedral core. CO and PPh_3 ligands have been omitted for clarity (blue, Co; yellow, Au; grey, C). Adapted with permission from ref.[78] Copyright 2014 American Chemical Society.

Ir–Mo vector have been isolated, which rapidly interconvert in solution.[67]

Positional isomerism of the CO and cyclopentadienyl ligands has been found in the crystal structures of three cluster compounds $[(\mu\text{-}H)Fe_2Mo(\mu_3\text{-}Te)(CO)_8Cp^*]$, $[FeMo_2(\mu_3\text{-}Te)(CO)_7Cp^*_2]$, and $[FeMoW(\mu_3\text{-}Te)(CO)_7CpCp^*]$ ($Cp = \eta^5\text{-}C_5H_5$, $Cp^* = \eta^5\text{-}C_5(CH_3)_5$).[68]

Just to conclude this Sections, the presence of organic ligands in MCCs may generate isomers in a further way, completely different from those discussed so far. Indeed, in all the examples presented above, the organic ligands retained their structures, and the isomers differed due to the coordination mode, coordination site, coordinated atoms, or orientation of the ligands. Conversely, in these last examples, the couples of isomers have the same atomic composition (as required by IUPAC),[35] but the ligands have different compositions. For instance, in the case of $[Co_4(CO)_6(C_7H_7)(C_7H_9)]$ and $[Co_4(CO)_6(C_8H_8)(C_6H_8)]$ (composition $C_{20}H_{16}Co_4O_6$),[69] the organic part of the cluster has composition $C_{14}H_{16}$, but in the former it results from one C_7H_7 and one C_7H_9 ring, whereas in the latter a

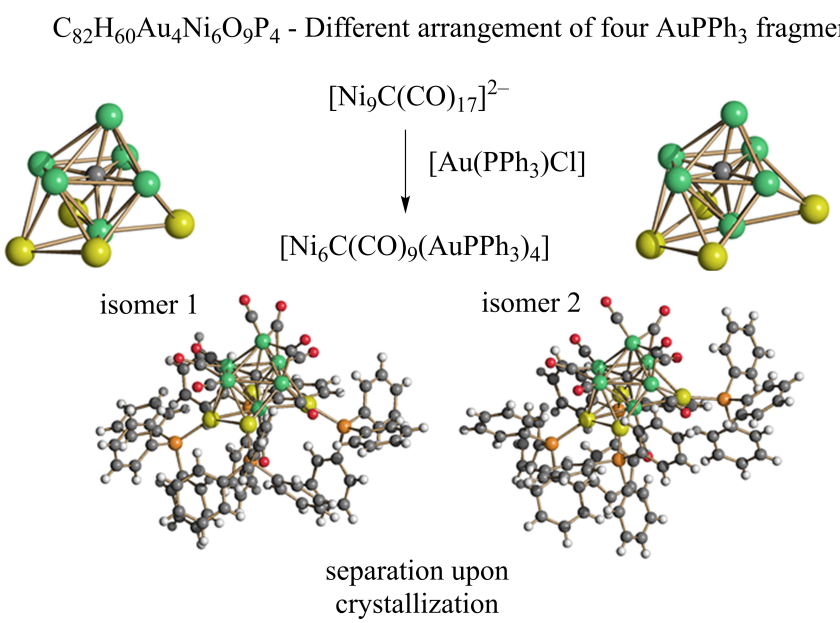

Figure 12. Surface isomerism – Different arrangement of $AuPPh_3$ fragments. Molecular structures of the two isomers of $[Ni_6C(CO)_9(AuPPh_3)_4]$ and their metal cores (green, Ni; yellow, Au; orange, P; red, O; grey, C; white, H). The two isomers have been structurally characterized as $[Ni_6C(CO)_9(AuPPh_3)_4]$·THF and $[Ni_6C(CO)_9(AuPPh_3)_4]$·THF·C_6H_{14} solvate crystals, respectively. Adapted with permission from Ref.[80] Copyright 2013 American Chemical Society.

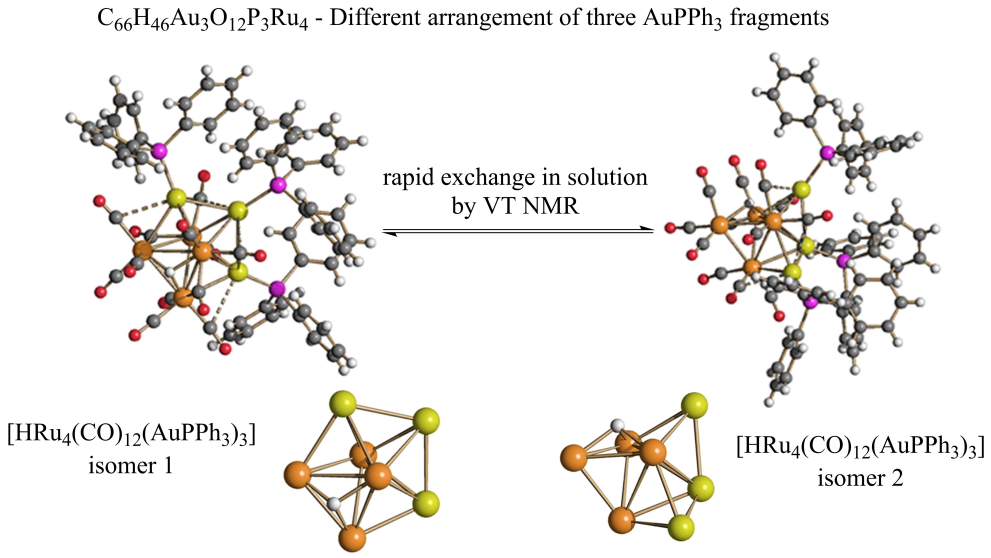

Figure 13. Surface isomerism – Different arrangement of $AuPPh_3$ fragments. Molecular structures of the two isomers of $[HRu_4(CO)_{12}(AuPPh_3)_3]$, differing for the disposition of the three $[AuPPh_3]^+$ fragments on the surface of the Ru_4 tetrahedron (orange, Ru; yellow, Au; green, P; red, O; grey, C; white, H).[81] Fragmented lines represent sub van der Waals Au···C(O) contacts, which are often present in heterometallic carbonyl clusters containing d^{10} M(I) (M=Cu, Ag, Au) centres. Their nature is rather debated, and details on this discussion may be found in the references.[78–81] Adapted from ref.[81] with permission from The Royal Society of Chemistry.

C_8H_8 and a C_6H_8 ligands are present (Scheme 3). Also $[H_2Os_3(CO)_9(C_6H_4)]$ and $[Os_3(CO)_9(C_6H_6)]$ have the same composition ($C_{15}H_6O_9Os_3$), but the latter contains a C_6H_6 ligand, whereas the former display one C_6H_4 and two hydrides.[70] These two isomers are somehow related by hydrogenation/dehydrogenation of the C_6-ring within the coordination sphere of the MCC.

A closely related example is represented by $[Os_3(\mu\text{-}H)(CO)_{10}\{\mu\text{-}\eta^2\text{-}ON{=}CPh_2\}]$ that thermally isomerizes to $[Os_3(CO)_{10}(\mu\text{-}OH)\{\mu\text{-}N{=}CPh_2\}]$ (composition of both isomers $C_{23}H_{11}N_1O_{11}Os_3$), which is formed by oxidative addition of the oxime with N–O bond cleavage (Figure 10).[71] A further case of isomerism generated by the structure of the organic ligands bonded to a MCC is $[Ru_6(\mu_5\text{-}C)(CO)_{14}(\mu\text{-}\eta^4\text{-}C_4H_4)\{\mu_3\text{-}C_2(CO_2Me)_2\}]$ and its isomer $[Ru_6(\mu_5\text{-}C)(CO)_{14}\{\mu_4\text{-}\eta^6\text{-}CHCHCHCC(CO_2Me)C\text{-}C(CO_2Me)\}(\mu\text{-}H)]$ (composition $C_{25}H_{10}O_{18}Ru_6$).[64] It must be remarked that in all these cases of structural isomerism comprising MCCs with the same compositions but different structures of the ligands, the two isomers may be or may be not related

Review
doi.org/10.1002/ejic.202400220

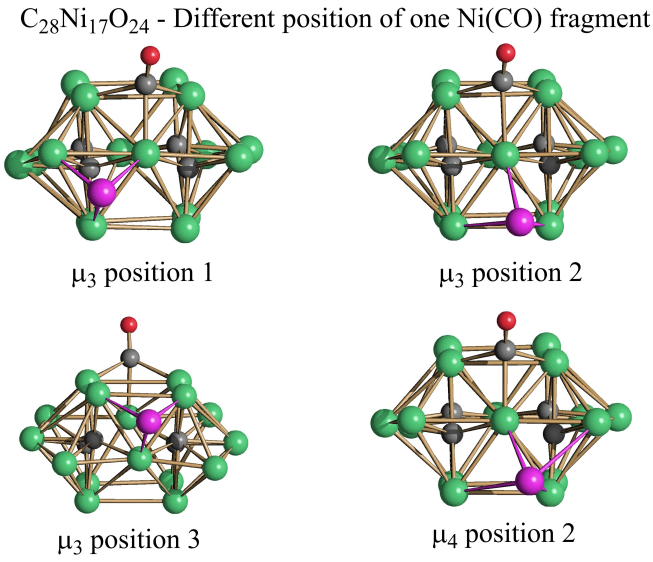

Figure 14. Surface isomerism – Different arrangement of a Ni(CO) fragment. The different capping modes of $[Ni_{16}(C_2)_2(CO)_{23}]^{4-}$ as found in the four $[Ni_{17}(C_2)_2(CO)_{24}]^{4-}$ isomers.[84] All CO ligands except μ_3-CO have been omitted for clarity. Capping Ni-atoms are in purple. See text for further details. Adapted from Ref.[84] with permission from The Royal Society of Chemistry.

by a direct mechanism. For instance, it is possible to convert $[Os_3(\mu\text{-H})(CO)_{10}\{\mu\text{-}\eta^2\text{-ON=CPh}_2\}]$ into $[Os_3(CO)_{10}(\mu\text{-OH})\{\mu\text{-N=CPh}_2\}]$ (Figure 10),[71] whereas $[Co_4(CO)_6(C_7H_7)(C_7H_9)]$ and $[Co_4(CO)_6(C_8H_8)(C_6H_8)]$ are obtained with different syntheses and cannot be interconverted (Scheme 3).[69]

Surface Isomerism Involving ML Fragments

The metal core of MCCs may coordinate M_mX_n fragments resulting in surface decorated MCCs.[25,27,31,72,73] These may be viewed as Lewis acid-base adducts, where often the M_mX_n fragment is the acid and the metal core of the cluster is the base. The metal fragments on the surface may be monometallic species such as Ni(CO), $Pt(PR_3)$, $Pd(PR_3)$, $[Au(PR_3)]^+$, CuX (X = Cl, Br, I), $[Cu(MeCN)]^+$, $[CdX]^+$ (X = Cl, Br, I), $InBr_3$, or larger fragments such as $[Au_2(P\text{–}P)]^{2+}$ (P–P = bidentate phosphine), $[Cd_2Cl_3]^+$, $[Cd_5(\mu\text{-Br})_5(dmf)_3]^{3+}$, $[In_2Br_5]^+$. There are also a few cases where the metal fragment behaves as a Lewis base, that is, $SnCl_2$, $[SnCl_3]^-$, $[Cl_2Sn(OH)SnCl_2]^-$, $[Cl_2SnOCOSnCl_2]^{2-}$.[74]

The metal fragments of surface decorated MCCs are somehow reminiscent of the staple motives decorating thiolate protected gold nanoclusters and related ligand protected precious metal molecular nanoclusters.[1–8] Therefore, the position and coordination mode of such metal fragments may originate isomers, as in the case of staple motives. From this point of view, MCCs decorated by $[Au(PR_3)]^+$ fragments are the most representative ones.[75,76] When two or more $[Au(PR_3)]^+$

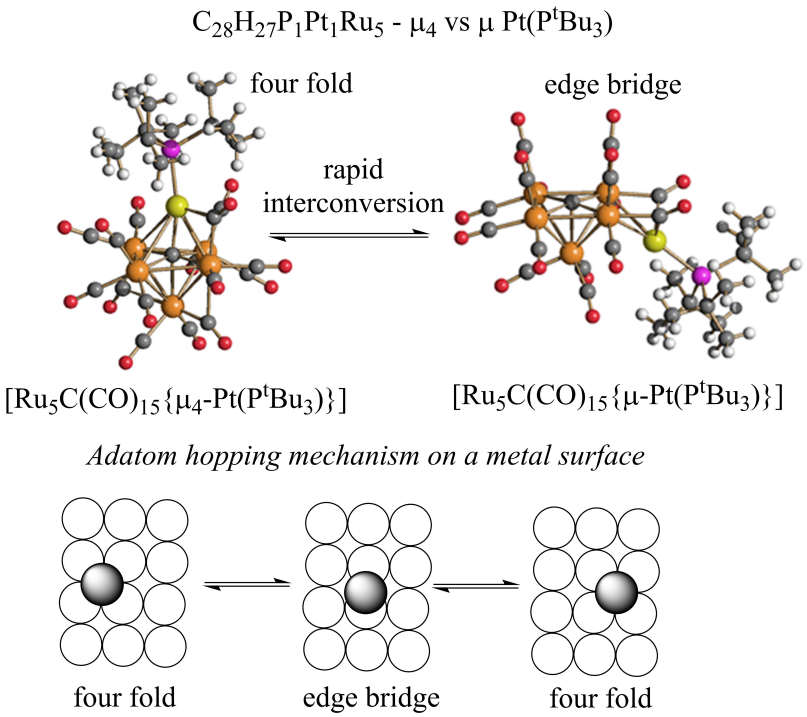

Figure 15. Surface isomerism – Different coordination of a $Pt(P^tBu_3)$ fragment. (Top) Molecular structures of the two isomers $[Ru_5C(CO)_{15}\{\mu_4\text{-}Pt(P^tBu_3)\}]$ and $[Ru_5C(CO)_{15}\{\mu\text{-}Pt(P^tBu_3)\}]$ (orange, Ru; yellow, Pt; green, P; red, O; grey, C; white, H). The two isomers rapidly interconvert in solution, mimicking the shift of a metal atom from a 4-fold to a 2-fold bonding site and back on a metal surface during the hopping process. (Bottom) A schematic representation of the adatom hopping mechanism on a metal surface. Empty circles represent the metal surface; the shaded circle represent the atom that moves. Adapted with permission from Ref.[86] Copyright 2003 American Chemical Society.

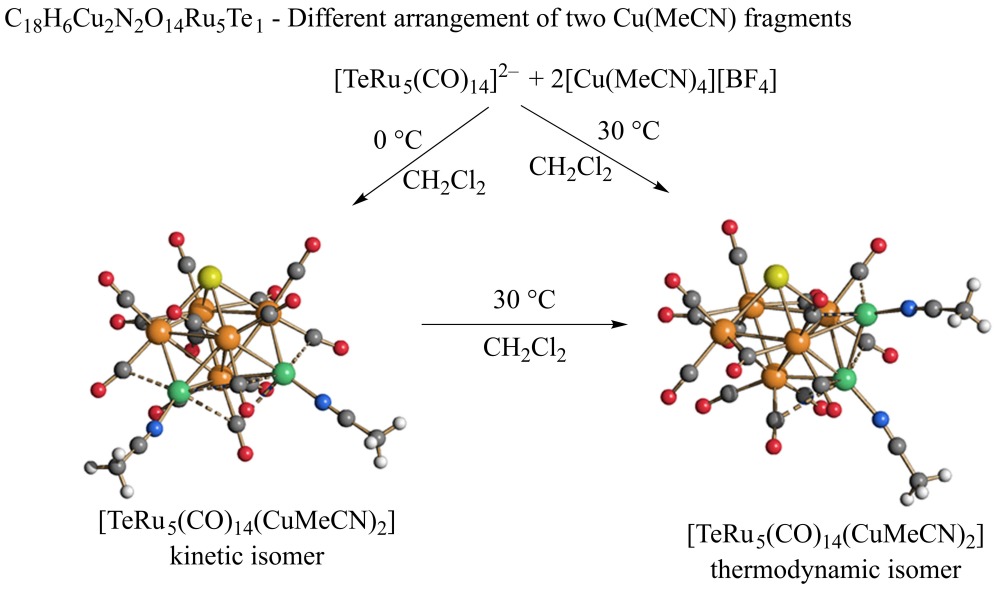

Figure 16. Surface isomerism – Different arrangement of two Cu(MeCN) fragments. Synthesis, thermal conversion and molecular structures of the two isomers $[TeRu_5(\mu\text{-}CO)_2(CO)_{12}(CuMeCN)_2]$ (kinetic isomer) and $[TeRu_5(\mu\text{-}CO)_3(CO)_{11}Cu_2(MeCN)_2]$ (thermodynamic isomer) (orange, Ru; yellow, Te; green, Cu; red, O; grey, C; white, H). Sub van der Waals Cu···C(O) contacts are represented as fragmented lines.[88]

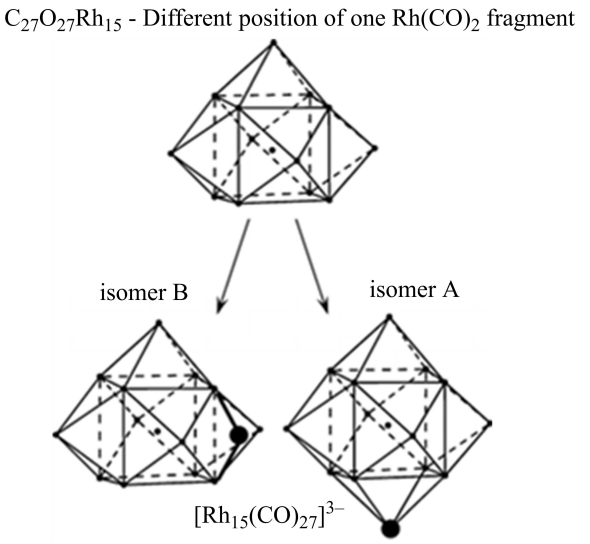

Figure 17. Surface isomerism – Different coordination of a $[Rh(CO)_2]^+$ fragment. The Rh_{15} metal cores of the two isomers of $[Rh_{15}(CO)_{27}]^{3-}$, resulting from the different capping mode of one $[Rh(CO)_2]^+$ fragment (Rh as a black circle) on the same pentacapped cubic body centred Rh_{14} kernel (top). Adapted with permission from Ref.[89] Copyright 2007 American Chemical Society.

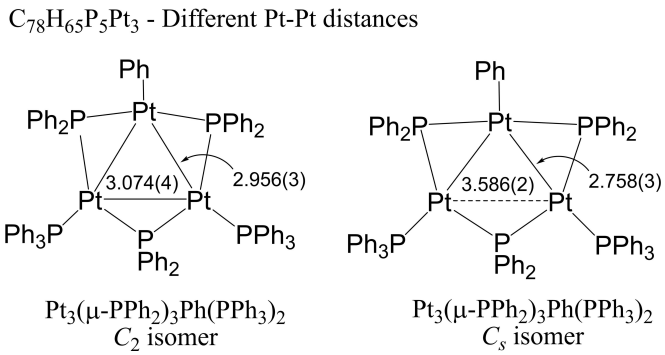

Figure 18. Core isomerism – Different Pt–Pt distances. Pt-triangle structure and chain-type structure of the two isomers of $[Pt_3(\mu\text{-}PPh_2)_3Ph(PPh_3)_2]$ showing different Pt–Pt bonding distances.[20–22]

fragments are present, isomers have been sometimes detected in solution by VT $^{31}P\{^1H\}$ NMR. For instance, two isomers have been spectroscopically characterized for both $[Os_6(CO)_{17}(Au_2dppm)_2]$ and $[Os_6(CO)_{17}(Au_2dppm)(AuPPh_3)_2]$.[77]

The structural characterization by SC-XRD of two or more isomers of the same MCCs differently decorated by $[Au(PR_3)]^+$ fragments is more rare. Three structural isomers have been characterized by SC-XRD in the case of $[Co_6C(CO)_{12}(AuPPh_3)_4]$ (Figure 11).[78] These are composed of the same octahedral $[Co_6C(CO)_{12}]^{4-}$ core decorated by four $[Au(PPh_3)]^+$ units, and the three isomers differ solely for the arrangement of such fragments. $[Co_6C(CO)_{12}(AuPPh_3)_4]$ is almost insoluble in all organic solvents and, after dissolution, it dissociates into $[Co_6C(CO)_{12}(AuPPh_3)_2]^{2-}$ and two $[Au(PPh_3)]^+$ fragments as indicated by VT $^{31}P\{^1H\}$ NMR spectroscopy. Thus, neutral $[Co_6C(CO)_{12}(AuPPh_3)_4]$ self-assembles upon crystallization and the structure of the resulting isomer is governed by a subtle balance of packing and van der Waals forces, as well as aurophilic and weak π–π and π–H interactions. Indeed, the three isomers have been found as three differently solvated crystals, that is, $[Co_6C(CO)_{12}(AuPPh_3)_4]$ (solvent-free), $[Co_6C(CO)_{12}(AuPPh_3)_4]\cdot THF$, and $[Co_6C(CO)_{12}(AuPPh_3)_4]\cdot 4THF$. All of them have been crystallized by layering n-hexane on a THF solution, and the resulting solid may contain one or a mixture of the three solvate crystals.

Two isomers, differing in the location of the three $[Au(PPh_3)]^+$ fragments, have been structurally characterized also in the case of $[Co_5C(CO)_{11}(AuPPh_3)_3]$.[79] In this case, one isomer has

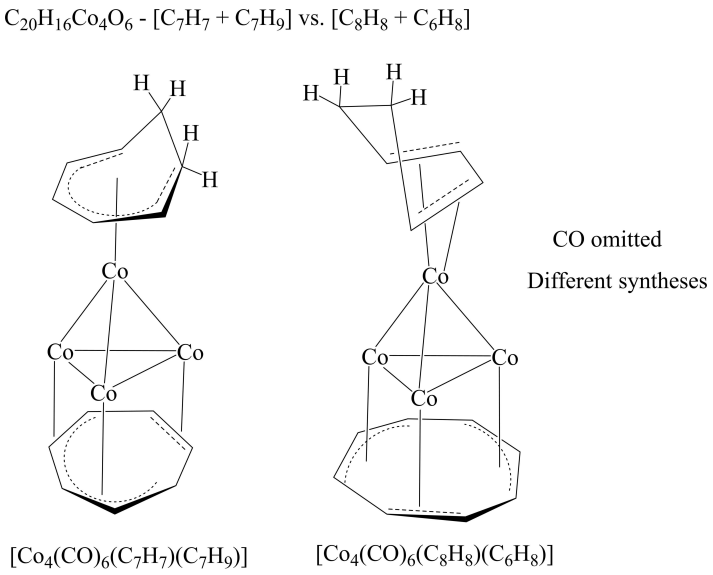

Scheme 3. Surface isomerism – Different structure of the organic ligands. The two isomers $[Co_4(CO)_6(C_7H_7)(C_7H_9)]$ and $[Co_4(CO)_6(C_8H_8)(C_6H_8)]$ have the same composition ($C_{20}H_{16}Co_4O_6$),[69] same structure of the metal core, same stereochemistry of the CO ligands (three terminal and three face capping), but different composition of the organic ligands.

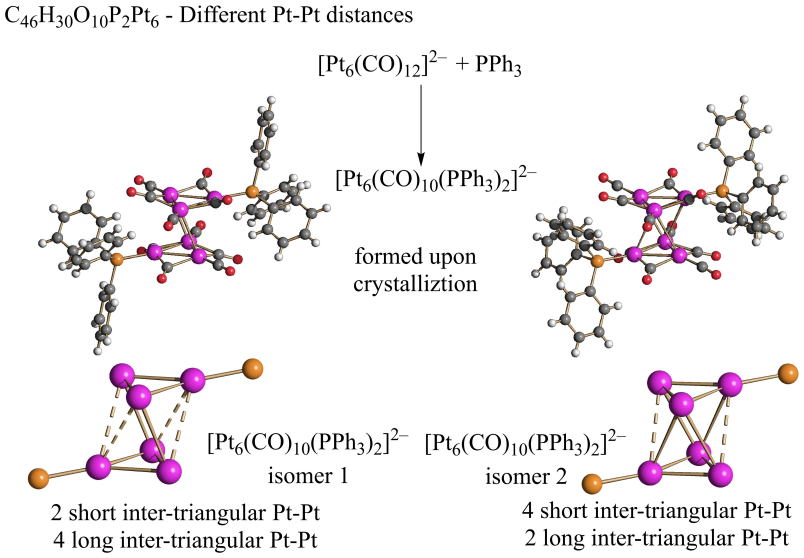

Figure 19. Core isomerism – Different Pt–Pt distances. Molecular structures of the two isomers of $[Pt_6(CO)_{10}(PPh_3)_2]^{2-}$ and their metal cores, as found in $[NBu_4]_2[Pt_6(CO)_{10}(PPh_3)_2]$ and $[NBu_4]_2[Pt_6(CO)_{10}(PPh_3)_2]\cdot 2THF$, respectively (Pt, purple; P, orange; C, grey, O, red; H, white; Pt–Pt < 3.22 Å full line, Pt–Pt > 3.22 Å fragmented line) The two isomers are formed upon crystallization of a solution containing $[Pt_6(CO)_{12}]^{2-}$ and PPh_3. Adapted with permission from Ref.[92] Copyright 2013 American Chemical Society.

been obtained from THF/n-hexane as $[Co_5C(CO)_{11}(AuPPh_3)_3]\cdot THF\cdot 0.5\ C_6H_{14}$ solvate crystals, and the second as $[Co_5C(CO)_{11}(AuPPh_3)_3]\cdot MeCN$ from MeCN/n-hexane/diisopropyl ether.

The reaction of $[Ni_9C(CO)_{17}]^{2-}$ with $[Au(PPh_3)Cl]$ affords $[Ni_6C(CO)_9(AuPPh_3)_4]$, which has been structurally characterized as the $[Ni_6C(CO)_9(AuPPh_3)_4]\cdot THF$ and $[Ni_6C(CO)_9(AuPPh_3)_4]\cdot THF\cdot C_6H_{14}$ solvate crystals (Figure 12).[80] The two solvates show some interesting differences concerning the weak Au···Au contacts among the four $[Au(PPh_3)]^+$ fragments on the surface of the cluster. DFT studies support the fact that the presence of the two isomers is related to solid-state packing effects. This corroborates the conclusion that Au···Au d^{10}–d^{10} interactions are rather soft and easily influenced by weak van der Waals forces because of the interaction of the cluster with the cocrystallized solvent molecules.

The reaction of $[HRu_4(CO)_{12}]^{3-}$ with three mole equivalents of $[Au(PPh_3)Cl]$ affords $[HRu_4(CO)_{12}(AuPPh_3)_3]$, which exists in solution as two rapidly exchanging isomers.[81] Both isomers have been structurally characterized by SC-XRD (Figure 13), and they are both based on the same Ru_4 tetrahedral core, differently decorated by three $AuPPh_3$ fragments. Also the stereo-

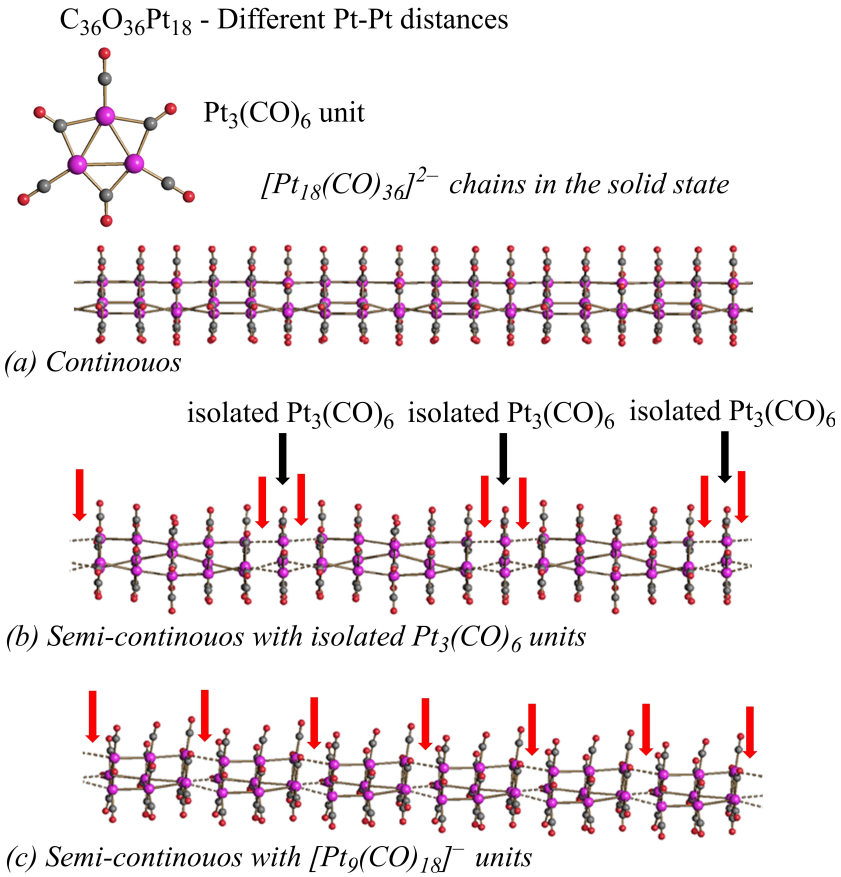

Figure 20. Core isomerism – Different Pt–Pt distances. Representation of the three isomeric chains of $[Pt_{18}(CO)_{36}]^{2-}$ anions as found in (a) $[Ru(bpy)_2(2\text{-PTZ})][Pt_{18}(CO)_{36}]$ and $[NMe_4]_2[Pt_{18}(CO)_{36}]\cdot 2CH_3COCH_3$ (continuous), (b) $[Ru(bpy)_3][Pt_{18}(CO)_{36}]$ (symmetric semi-continuous with isolated $Pt_3(CO)_6$ units), and (c) $[Ph_3P(CH_2)_{12}PPh_3][Pt_{18}(CO)_{36}]$ (semi-continuous based on an infinite chain of $[Pt_9(CO)_{18}]^{-}$ anions) (Pt, purple; C, grey, O, red; Pt–Pt < 3.22 Å full line, Pt–Pt > 3.22 Å fragmented line). Red arrows have been added in correspondence of longer Pt–Pt contacts (> 3.22 Å), whereas black arrows indicate isolated $Pt_3(CO)_6$ units in (b).[93–96] Adapted from Ref.[96] with permission from Elsevier.

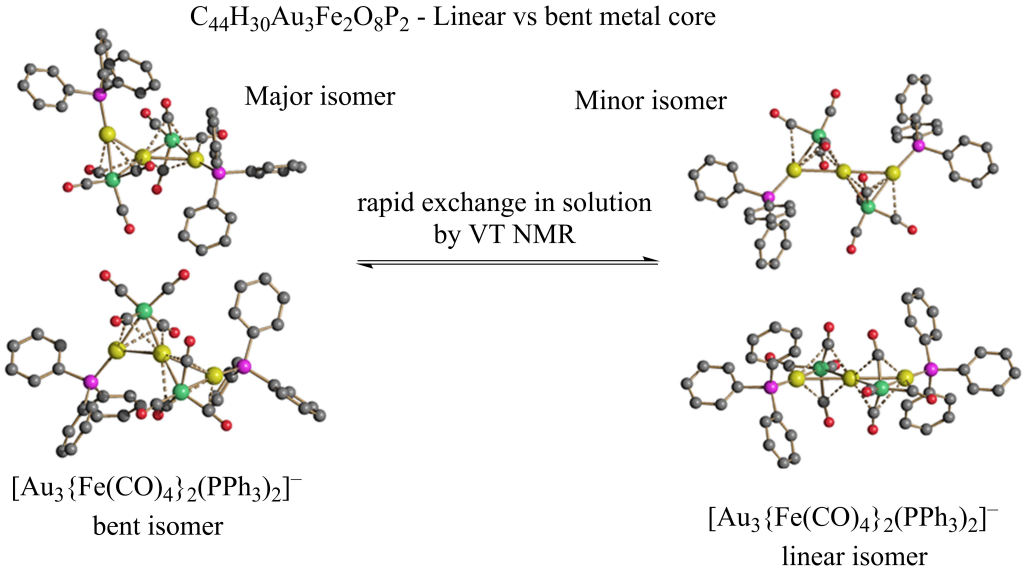

Figure 21. Core isomerism – Different structure of the $[Au_3]^{3+}$ core. Two views of the molecular structures of the two isomers of $[Au_3\{Fe(CO)_4\}_2(PPh_3)_2]^{-}$ (green Fe; yellow Au; purple P; blue N; red O; grey C). H-atoms have been omitted for clarity. The two isomers were present within the crystal of $[Au(IMes)_2][Au_3\{Fe(CO)_4\}_2(PPh_3)_2]\cdot 0.67CH_2Cl_2$ in the ratio major: minor = 2: 1. Adapted with permission from Ref.[98] Copyright 2020 American Chemical Society.

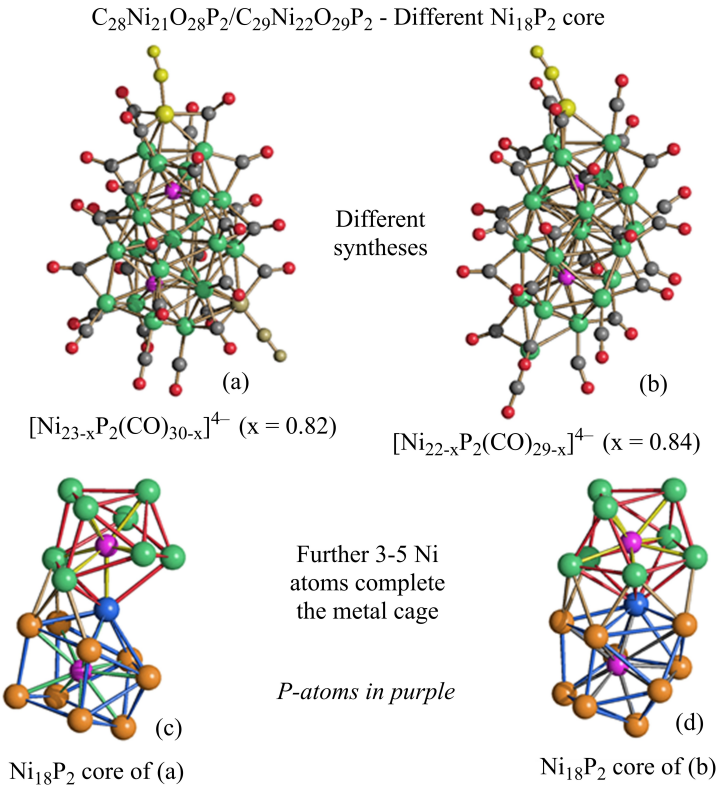

Figure 22. Core isomerism – Different structure of the $Ni_{18}P_2$ framework. The molecular structures of (a) $[Ni_{23-x}P_2(CO)_{30-x}]^{4-}$ (x = 0.82) (yellow, Ni(CO) fragment with 0.50 occupancy factor; olive green, Ni(CO) fragment with 0.68 occupancy factor) and (b) $[Ni_{22-x}P_2(CO)_{29-x}]^{4-}$ (x = 0.84) (yellow, Ni(CO) fragment with 0.16 occupancy factor) (green, Ni; purple, P; grey, C; red, O). (c) The $Ni_{18}P_2$ framework of $[Ni_{23-x}P_2(CO)_{30-x}]^{4-}$ (x = 0.82) obtained by the condensation via a vertex (in blue) of a Ni_9P mono-capped square anti-prism (Ni atoms in green, Ni–Ni bonds in red, Ni–P bonds in yellow) and a $Ni_{10}P$ sphenocorona (Ni atoms in orange, Ni–Ni bonds in blue, Ni–P bonds in green). (d) The $Ni_{18}P_2$ framework of $[Ni_{22-x}P_2(CO)_{29-x}]^{4-}$ (x = 0.84) obtained by the condensation via a vertex (in blue) of a Ni_9P mono-capped square anti-prism (Ni atoms in green, Ni–Ni bonds in red, Ni–P bonds in yellow) and a $Ni_{10}P$ bi-capped square anti-prism (Ni atoms in orange, Ni–Ni bonds in blue, Ni–P bonds in grey). Adapted with permission from Ref.[85] Copyright 2020 American Chemical Society.

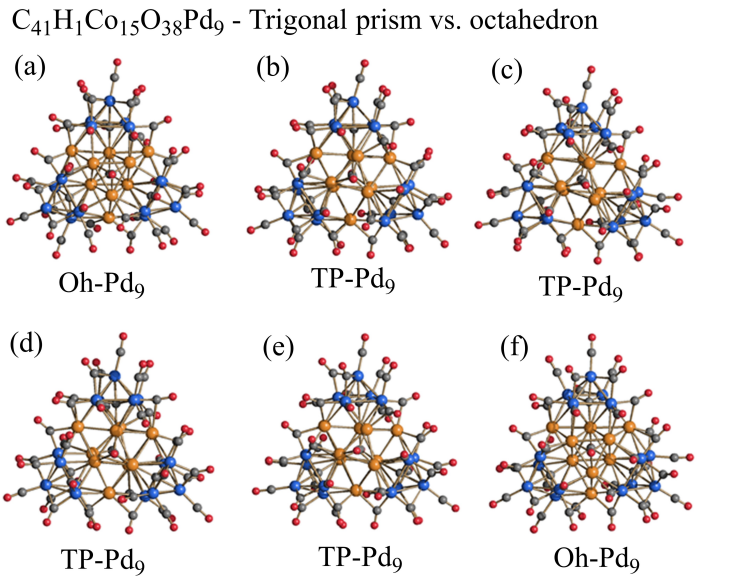

Figure 23. Core isomerism – Different structure of the Pd_9 core. Molecular structures of the $[HCo_{15}Pd_9C_3(CO)_{38}]^{2-}$ anion as found in: $[NMe_3(CH_2Ph)]_2[HCo_{15}Pd_9C_3(CO)_{38}]\cdot CH_2Cl_2$, (a) Oh-$Pd_9$ isomer and (b) TP-Pd_9 isomer (isomer ratio within the crystal 1 : 1); (c) $[NMe_3(CH_2Ph)]_2[HCo_{15}Pd_9C_3(CO)_{38}]\cdot 2CH_2Cl_2$ TP-Pd_9 isomer; (d) $[NEt_3(CH_2Ph)]_2[HCo_{15}Pd_9C_3(CO)_{38}]\cdot CH_2Cl_2$, TP-$Pd_9$ isomer; (e) $[MePPh_3]_2[HCo_{15}Pd_9C_3(CO)_{38}]\cdot 2.5CH_2Cl_2$, TP-$Pd_9$ isomer; (f) $[MePPh_3]_2[HCo_{15}Pd_9C_3(CO)_{38}]$, Oh-$Pd_9$ isomer (orange, Pd; blue, Co; red, O; grey; C; TP=Trigonal Prism; Oh=Octahedron).[99,100] Adapted with permission from Ref.[99] Copyright 2020 American Chemical Society.

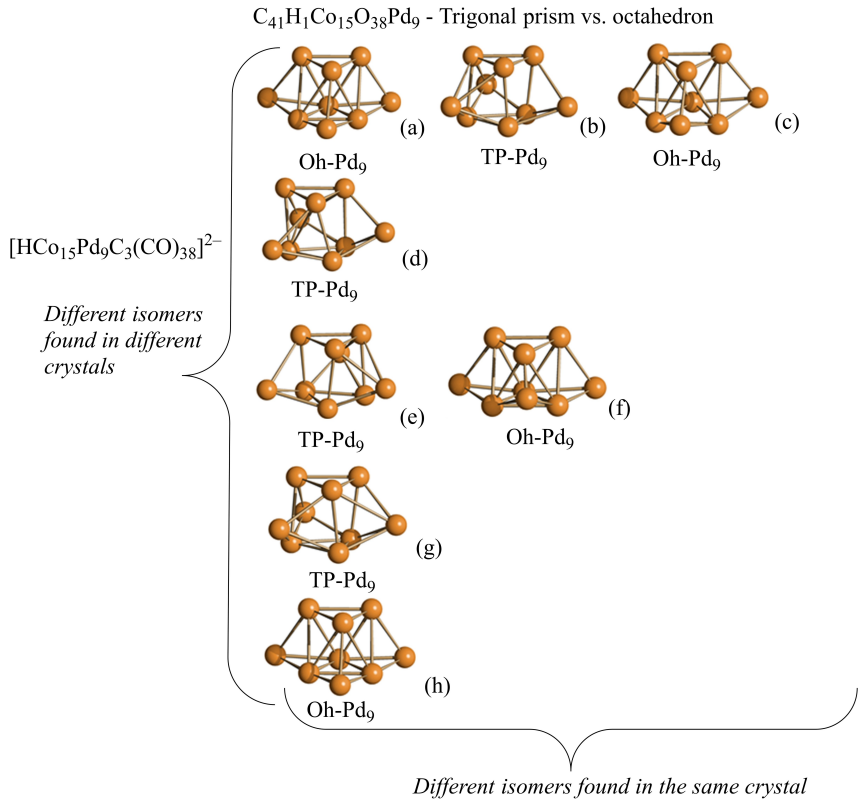

Figure 24. Core isomerism – Different structure of the Pd_9 core. The Pd_9 core of $[HCo_{15}Pd_9C_3(CO)_{38}]^{2-}$ as found in different salts. The structures in the same line have been found within the same single crystal. $[NMe_3(CH_2Ph)]_2[HCo_{15}Pd_9C_3(CO)_{38}]\cdot CH_2Cl_2$ (two independent molecules are present within the unit cell): (a) Oh-Pd_9 isomer (molecule 1), (b) TP-Pd_9 isomer (91 % of molecule 2), (c) Oh-Pd_9 isomer (9 % of molecule 2). $[NMe_3(CH_2Ph)]_2[HCo_{15}Pd_9C_3(CO)_{38}]\cdot 2CH_2Cl_2$: (d) TP-$Pd_9$ isomer. $[NEt_3(CH_2Ph)]_2[HCo_{15}Pd_9C_3(CO)_{38}]\cdot CH_2Cl_2$: (e) TP-$Pd_9$ isomer (94 %), (f) Oh-Pd_9 isomer (6 %). $[MePPh_3]_2[HCo_{15}Pd_9C_3(CO)_{38}]\cdot 2.5CH_2Cl_2$: (g) TP-$Pd_9$ isomer. $[MePPh_3]_2[HCo_{15}Pd_9C_3(CO)_{38}]$: (h) Oh-$Pd_9$ isomer.[99,100] Adapted with permission from Ref.[99] Copyright 2020 American Chemical Society.

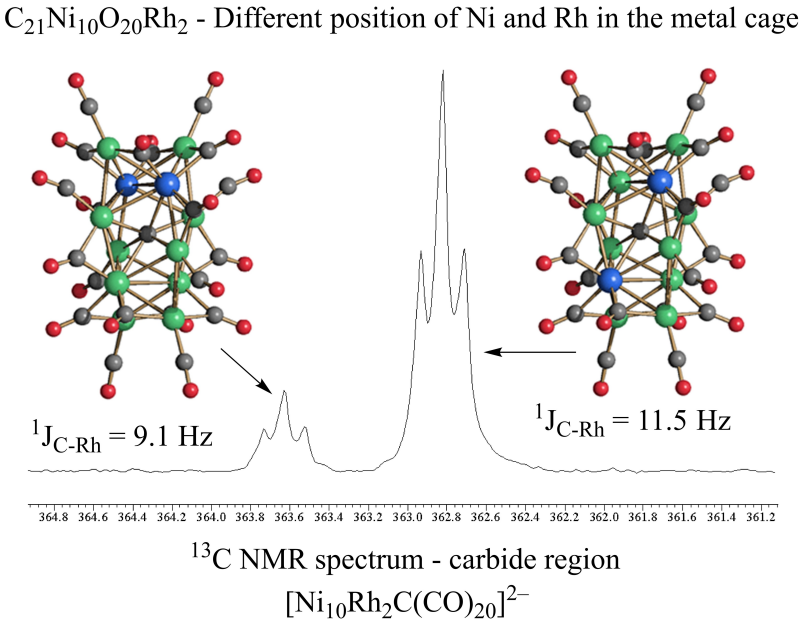

Figure 25. Core isomerism – Different position of Ni and Rh atoms within the metal kernel. The two cocrystallyzed isomers of $[Ni_{10}Rh_2C(CO)_{20}]^{2-}$ and their ^{13}C NMR spectrum in d^6-acetone at 298 K (blue, Rh; green, Ni; grey, C; red, O). Adapted from Ref.[110] with permission from Wiley.

chemistry of the CO ligands is slightly different, since, disregarding weak Au···C(O) contacts, one isomer contains only terminal carbonyls, whereas the second one displays ten terminal and two edge-bridging CO ligands.

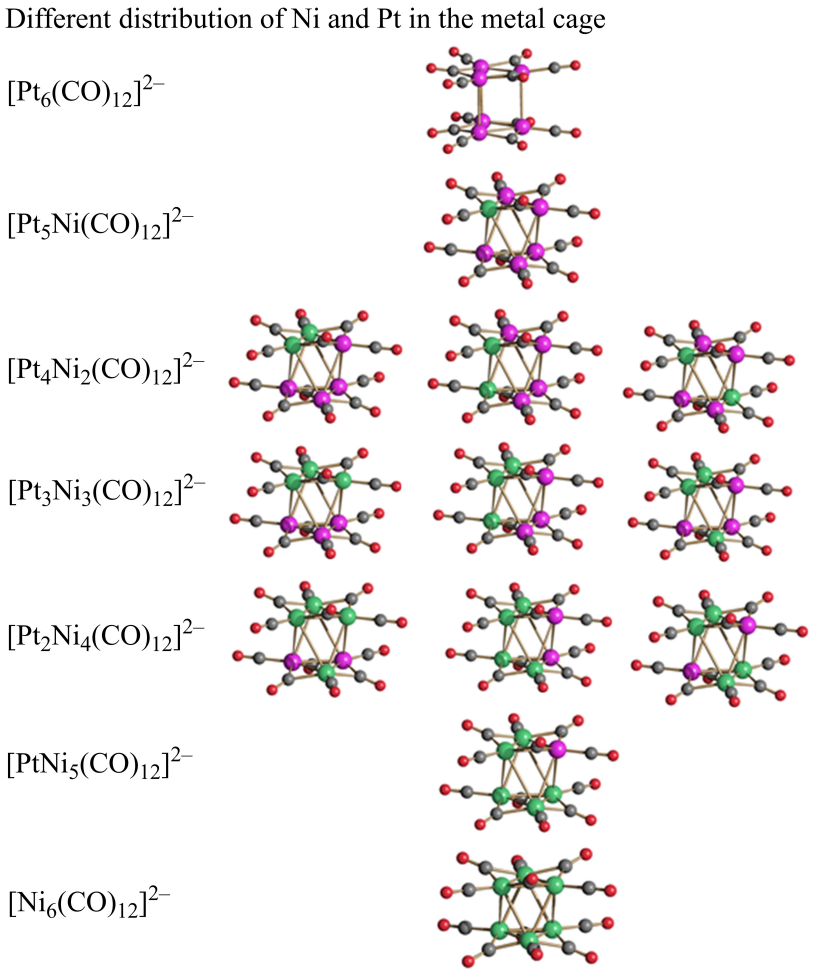

Figure 26. Core isomerism – Different distribution of Ni and Pt within the metal kernel. All possible isomers of the $[Pt_{6-x}Ni_x(CO)_{12}]^{2-}$ (x = 0–6) molecular alloy clusters (purple, Pt; green, Ni; grey, C; red, O). Mixtures of isomers and species with different compositions are always found in the solid state and in solution. All these species display an octahedral metal cage, except $[Pt_6(CO)_{12}]^{2-}$ that adopts a trigonal prismatic structure. Adapted with permission from Ref.[114] Copyright 2021 American Chemical Society.

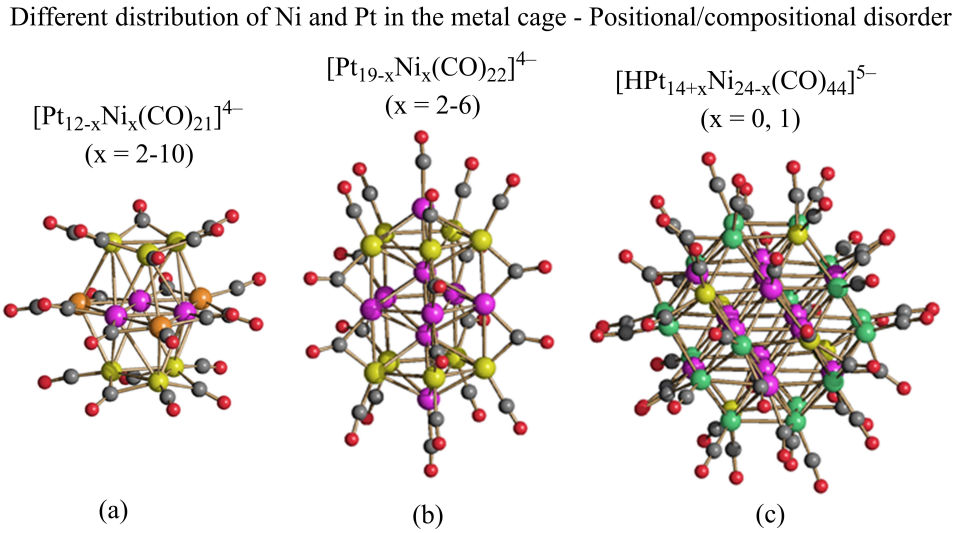

Figure 27. Core isomerism – Ni/Pt positional (and compositional) disorder (alloy cluster). Molecular structures of (a) $[Pt_{12-x}Ni_x(CO)_{21}]^{4-}$ (x = 2–10), (b) $[Pt_{19-x}Ni_x(CO)_{22}]^{4-}$ (x = 2–6), and (c) $[HPt_{14+x}Ni_{24-x}(CO)_{44}]^{5-}$ (x = 0, 1) (orange and yellow, disordered Ni/Pt with different occupancy factors; green, Ni; purple, Pt; red, O; grey, C). Some metal positions display Ni/Pt disorder (orange and yellow) that may originate mixtures of isomers. In addition to positional disorder, also compositional disorder is present. Thus, these alloy clusters are actually mixtures of isomers with the same metal compositions as well as clusters with different Ni/Pt content. Adapted from Ref.[119] with permission from The Royal Society of Chemistry.

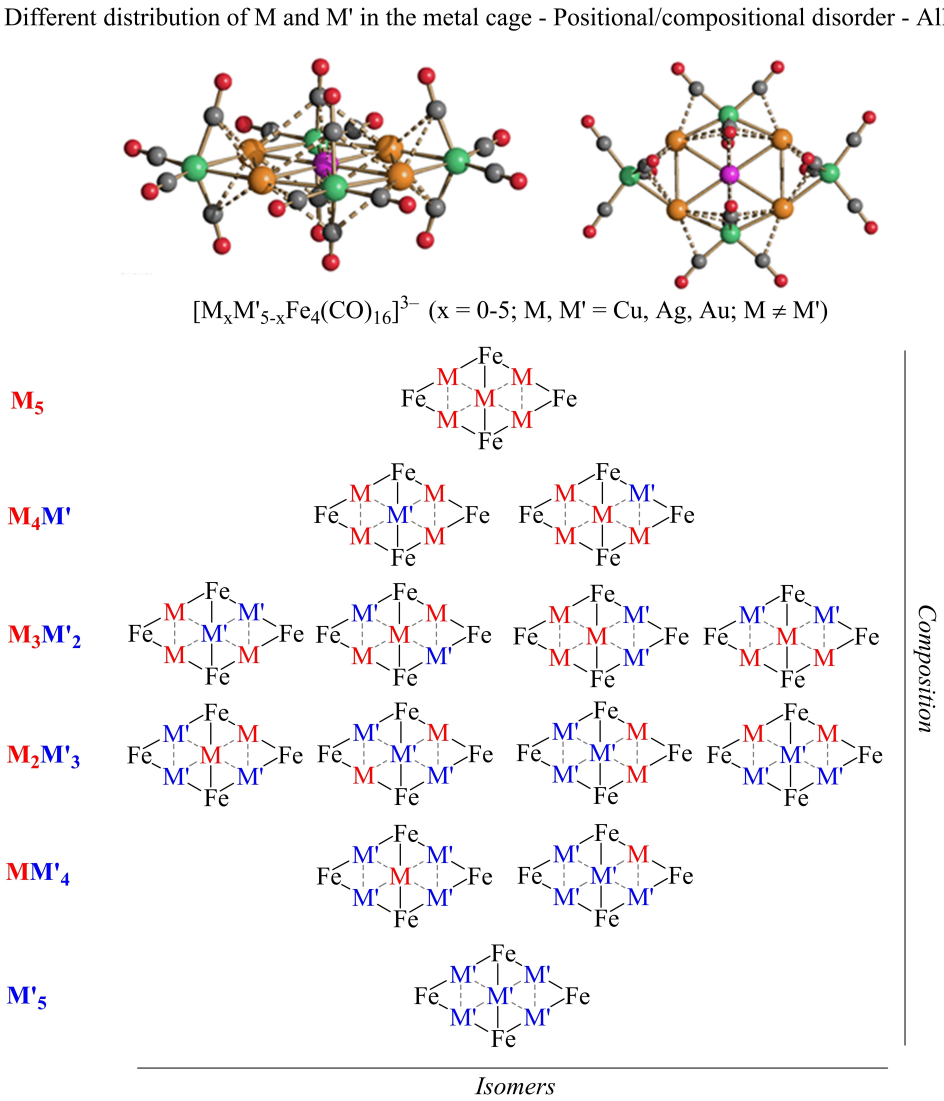

Figure 28. Core isomerism – M/M′ positional (and compositional) disorder (alloy cluster). (top) Molecular structure of the $[M_xM'_{5-x}Fe_4(CO)_{16}]^{3-}$ (x = 0–5; M, M′ = Cu, Ag, Au; M ≠ M′) clusters (purple, M in the centre; orange, M in the corner positions; green, Fe; grey, C; red, O). M–C(O) contacts are represented as fragmented lines. (bottom) Isomers are originated due to different distributions of M and M′ between the central and corner positions. Mixtures of isomers and clusters with different compositions are present in solution and in the solid state. The exact composition depends on the experimental conditions adopted during synthesis. Adapted with permission from Ref.[120] Copyright 2020 American Chemical Society.

Structural isomerism has been proved by SC-XRD also for MCCs containing other 12 electrons ML fragments, that is Ni(CO), $Pt(PR_3)$, $Pd(PR_3)$, and $[Cu(MeCN)]^+$. Capping a triangular face of a MCC with a 12 electron ML fragment does not alter the electron count of the cluster.[82] Because of this, several MCCs differing solely for the addition/removal of a few Ni(CO) fragments are known.[83] For the same reason, isomers may originate due to the different location of a Ni(CO) fragment around the same MCC core. This point is well exemplified by $[Ni_{16}(C_2)_2(CO)_{23}]^{4-}$ and the four isomers of $[Ni_{17}(C_2)_2(CO)_{24}]^{4-}$ (Figure 14).[84] These clusters possess the same square orthobicupola Ni_{16} core with two fully interstitial C_2 acetylide units. Addition of one Ni(CO) fragments on different triangular faces of $[Ni_{16}(C_2)_2(CO)_{23}]^{4-}$ affords the four different isomers of $[Ni_{17}(C_2)_2(CO)_{24}]^{4-}$, which may be viewed as snapshots of the possible rambling around the Ni_{16} square orthobicupola of the additional Ni(CO) fragment. It must be remarked that all four isomers have been structurally characterized within two crystal solvates, that is, $[NEt_4]_4[Ni_{16+x}(C_2)_2(CO)_{23+x}]$ (x = 0.12) and $[NEt_4]_4[Ni_{16+x}(C_2)_2(CO)_{23+x}]\cdot 1.33CH_3COCH_3$ (x = 0.96). Both crystal structures contain one Ni(CO) fragment with partial occupancy factor and, thus, they actually contain mixtures of $[Ni_{16}(C_2)_2(CO)_{23}]^{4-}$ and $[Ni_{17}(C_2)_2(CO)_{24}]^{4-}$. One single isomer of $[Ni_{17}(C_2)_2(CO)_{24}]^{4-}$ is present within $[NEt_4]_4[Ni_{16+x}(C_2)_2(CO)_{23+x}]$ (x = 0.12), whereas the other three isomers have been found in the crystal structure of $[NEt_4]_4[Ni_{16+x}(C_2)_2(CO)_{23+x}]\cdot 1.33CH_3COCH_3$ (x = 0.96).

A similar phenomenon has been found in the crystals of $[NEt_4]_4[Ni_{23-x}P_2(CO)_{30-x}]\cdot 2CH_3COCH_3$ (x = 0.82), which actually contain a mixture of $[Ni_{23}P_2(CO)_{30}]^{4-}$, $[Ni_{22}P_2(CO)_{29}]^{4-}$ (two isomers differing for the location of a Ni(CO) fragment), and

Review
doi.org/10.1002/ejic.202400220

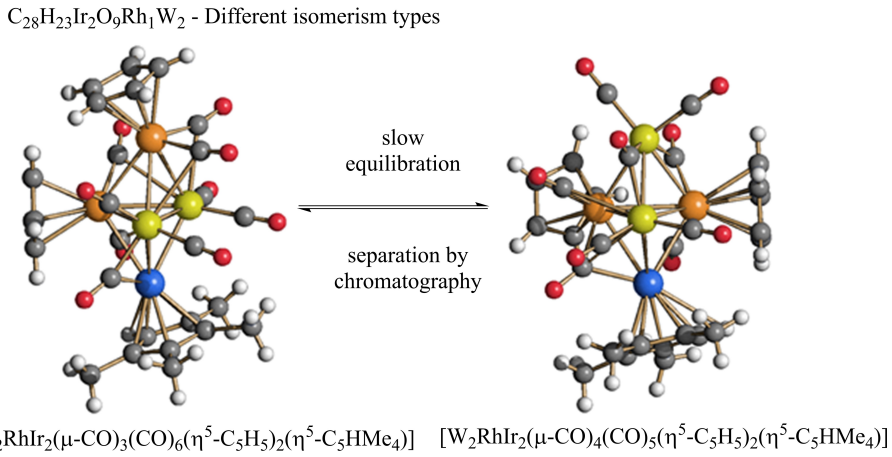

Figure 29. Core isomerism – Dynamic permutational isomerism. Molecular structures of the two isomers $[W_2RhIr_2(\mu\text{-}CO)_3(CO)_6(\eta^5\text{-}C_5H_5)_2(\eta^5\text{-}C_5HMe_4)]$ and $[W_2RhIr_2(\mu\text{-}CO)_4(CO)_5(\eta^5\text{-}C_5H_5)_2(\eta^5\text{-}C_5HMe_4)]$ (orange, W; yellow, Ir; blue, Rh; red, O; grey, C; white, H). The isomers differ for a combination of causes: position of metal atoms, position of the ligands, stereochemistry of CO ligands.[121]

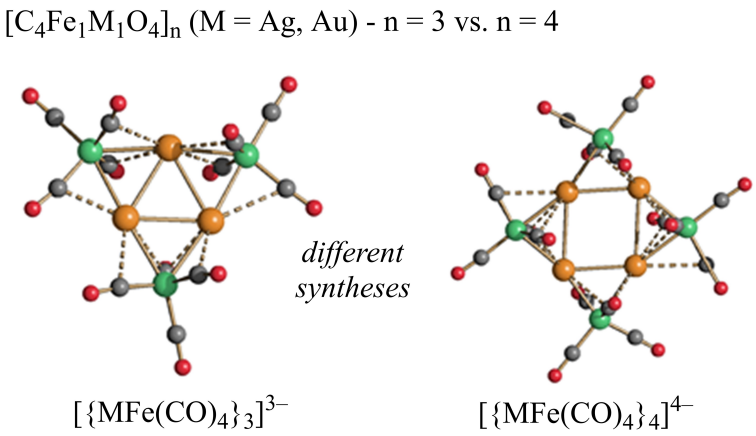

Figure 30. Polymerization isomerism – Trimeric and tetrameric structures of the same unit formula. Molecular structures of the $[\{MFe(CO)_4\}_3]^{3-}$ trimer and $[\{MFe(CO)_4\}_4]^{4-}$ tetramer (M=Ag, Au) (orange, Ag or Au; green, Fe; grey, C; red, O). Sub Van der Waals M···C(O) contacts are represented as fragmented lines. The trimer has been obtained from the reaction of Collman's reagent $Na_2[Fe(CO)_4]\cdot 2thf$ with two equivalents of M(IMes)Cl (IMes = $C_3N_2H_2(C_6H_2Me_3)_2$; M=Ag, Au), whereas the $[\{MFe(CO)_4\}_4]^{4-}$ tetramer has been obtained from the 1: 1 reaction of $Na_2[Fe(CO)_4]\cdot 2thf$ with $AgNO_3$ or $Au(Et_2S)Cl$. Adapted with permission from Ref.[123] Copyright 2019 American Chemical Society.

$[Ni_{21}P_2(CO)_{28}]^{4-}$, because of the presence of two Ni(CO) fragments with partial occupancy factors (0.68 and 0.50).[85]

The reaction of $[Ru_5C(CO)_{15}]$ with $[Pt(P^tBu_3)_2]$ affords $[Ru_5C(CO)_{15}\{Pt(P^tBu_3)\}]$ that exists in solution as two interconverting isomers as demonstrated by VT $^{31}P\{^1H\}$ NMR spectroscopy. The first isomer, $[Ru_5C(CO)_{15}\{\mu_4\text{-}Pt(P^tBu_3)\}]$, has been crystallized from benzene/octane, and the second one, $[Ru_5C(CO)_{15}\{\mu\text{-}Pt(P^tBu_3)\}]$, form diethyl ether.[86] Both isomers are based on the same Ru_5C square pyramid and differ for the location of the $Pt(P^tBu_3)$ fragment (Figure 15). This caps the square face of $[Ru_5C(CO)_{15}]$ in the isomer $[Ru_5C(CO)_{15}\{\mu_4\text{-}Pt(P^tBu_3)\}]$, resulting in a Ru_5PtC octahedron. Conversely, the $Pt(P^tBu_3)$ fragment bridges one Ru–Ru edge of the square base of $Ru_5C(CO)_{15}$ in the isomer $[Ru_5C(CO)_{15}\{\mu\text{-}Pt(P^tBu_3)\}]$. The interconversion mechanism involves the reversible breaking and making of two of the Pt–Ru bonds with a shift of the Pt-phosphine grouping back and forth between the 4-fold Ru_4 site and the 2-fold edge-bridging Ru_2 site. The interconversion of the two isomers could be viewed as one of the elementary steps of the adatom hopping mechanism occurring on a metal surface.

Similarly, two isomers, that is, $[Ru_6C(CO)_{17}\{\mu\text{-}Pd(P^tBu_3)\}_2]$ and $[Ru_6C(CO)_{17}\{\mu\text{-}Pd(P^tBu_3)\}\{\mu_3\text{-}Pd(P^tBu_3)\}]$, have been isolated and characterized by SC-XRD upon reaction of $[Ru_6C(CO)_{17}]$ with $[Pd(P^tBu_3)_2]$.[87] In the former, both $Pd(P^tBu_3)$ groups are on bridging positions around the Ru_6C octahedron, whereas in the latter isomer, one $Pd(P^tBu_3)$ is edge bridging and the other face capping.

The two isomers $[TeRu_5(\mu\text{-}CO)_2(CO)_{12}(CuMeCN)_2]$ (kinetic isomer) and $[TeRu_5(\mu\text{-}CO)_3(CO)_{11}Cu_2(MeCN)_2]$ (thermodynamic isomer) have been obtained from the reaction of $[TeRu_5(CO)_{14}]^{2-}$ with two mole equivalents of $[Cu(MeCN)_4][BF_4]$ in CH_2Cl_2 at 0 °C and 30 °C, respectively (Figure 16).[88] The kinetic isomer is converted into the thermodynamic one upon heating in CH_2Cl_2 at 30 °C. Both structures contain a $TeRu_5$ octahedron differently capped by two Cu(MeCN) fragments. A weak cuprophilic Cu···Cu interaction is present in the thermodynamic isomer, but

Review
doi.org/10.1002/ejic.202400220

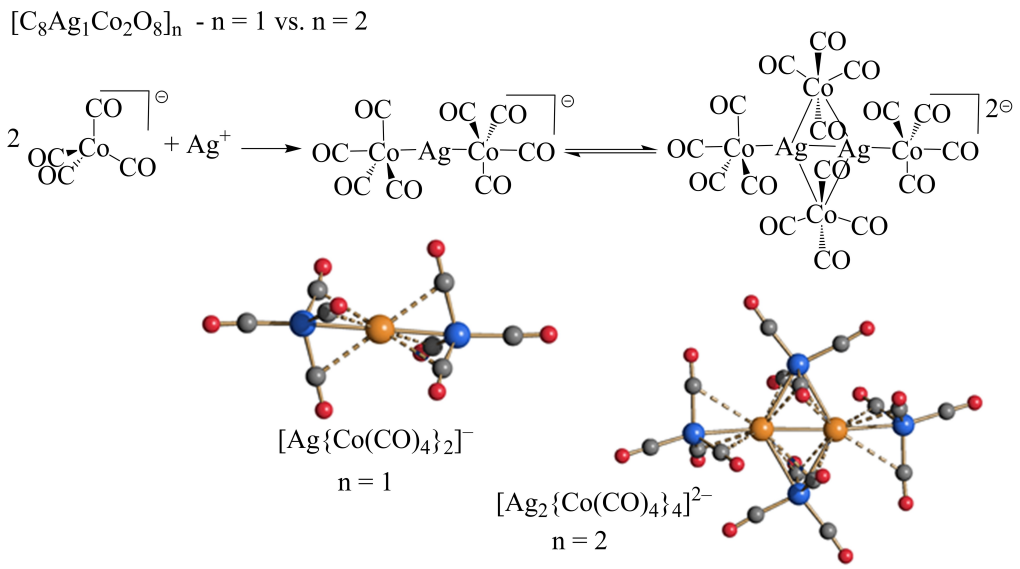

Figure 31. Polymerization isomerism – Monomeric and dimeric structures of the same unit formula. Equilibrium between the $[Ag\{Co(CO)_4\}_2]^-$ monomer and the $[Ag_2\{Co(CO)_4\}_4]^{2-}$ dimer. The monomer is formed in solution upon mixing Ag^+ and $[Co(CO)_4]^-$ in a 1 : 2 ratio. Depending on the crystallization conditions, the monomer or the dimer may be found in the solid state. Sub Van der Waals Ag···C(O) contacts are represented as fragmented lines (orange, Ag; blue, Co; red, O; grey, C).[45]

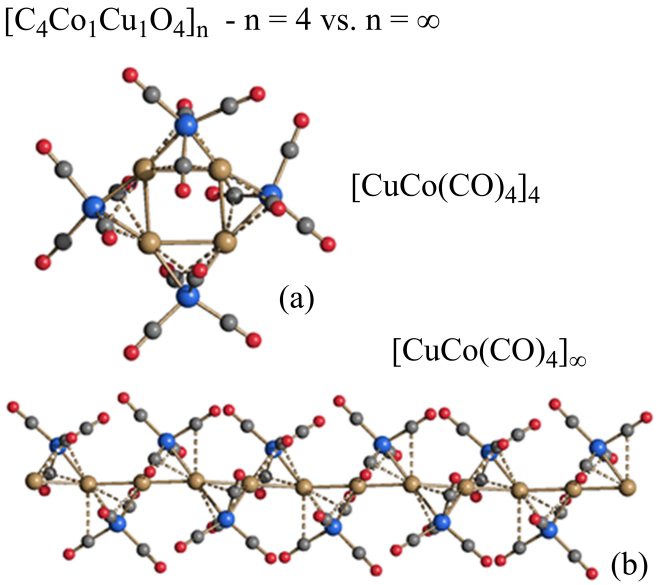

Figure 32. Polymerization isomerism – Tetrameric and polymeric structures of the same unit formula. The molecular structures of the $[CuCo(CO)_4]_4$ tetramer, and the $[CuCo(CO)_4]_\infty$ infinite polymer (brown, Cu; blue, Co; red, O; grey, C). Sub Van der Waals Cu···C(O) contacts are represented as fragmented lines.[125,126]

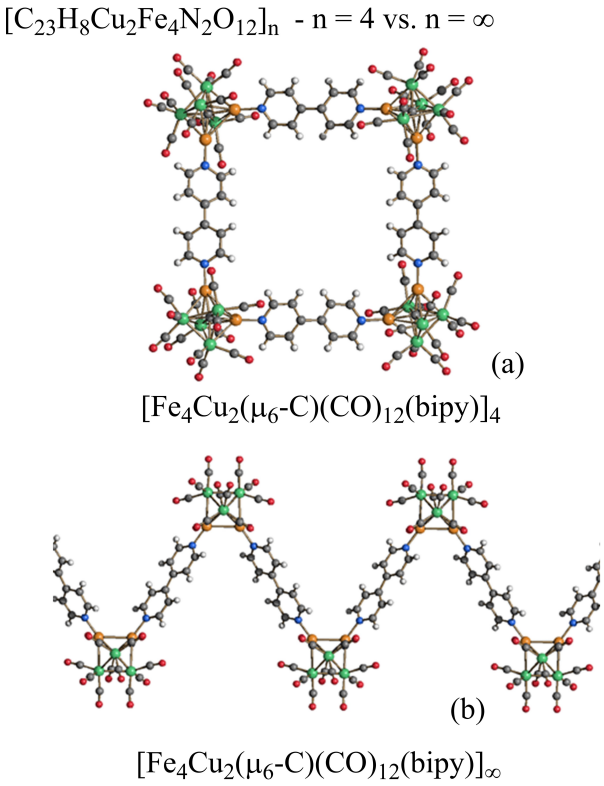

Figure 33. Polymerization isomerism – Tetrameric and polymeric structures of the same unit formula. The molecular structures of (a) the $[Fe_4Cu_2(\mu_6\text{-}C)(CO)_{12}(bipy)]_4$ tetramer and (b) a chunk of the infinite zig-zag chain polymer $[Fe_4Cu_2(\mu_6\text{-}C)(CO)_{12}(bipy)]_\infty$ (green, Fe; orange, Cu; blue, N; red, O; grey, C; white, H). Adapted from Ref.[127] with permission from The Royal Society of Chemistry.

not in the kinetic isomer. Some minor differences in the stereochemistry of the carbonyls are also present.

Finally, two isomers differing for the location of one 12 electrons $[Rh(CO)_2]^+$ fragment on the cluster surface have been structurally characterized for $[Rh_{15}(CO)_{27}]^{3-}$ (Figure 17).[89] Both isomers are based on the same body centred cubic Rh_9 core capped on five square faces by five further Rh atoms, as found in $[Rh_{14}(CO)_{25}]^{4-}$. In the first isomer (A), the $[Rh(CO)_2]^+$ fragment is located on the sixth square face of the cubic core, whereas it is located on a concave face generated by two Rh atoms capping two adjacent square faces of the Rh-centered cube in

the second isomer (B). It must be remarked that, in this case, the two isomers have been obtained by different reaction pathways. Thus, the first isomer of $[Rh_{15}(CO)_{27}]^{3-}$ (A) has been obtained by the chemical oxidation of $[Rh_7(CO)_{16}]^{3-}$, whereas the second isomer (B) has been synthesized upon pyrolysis of $Rh_4(CO)_{12}$ in ^{i}PrOH in the presence of NaOH.

Core Isomerism

Core Isomerism Involving M–M Distances

The first example of cluster core isomerism involving M–M distances is represented by $[Pt_3(\mu\text{-}PPh_2)_3Ph(PPh_3)_2]$ (Figure 18).[20–22] Even if this is not a MCC, it will be briefly discussed herein in order to introduce this phenomenon, before showing some examples concerning MCCs. The first isomer of $[Pt_3(\mu\text{-}PPh_2)_3Ph(PPh_3)_2]$ possesses C_2 symmetry and may be described as a Pt_3 isosceles triangle with two slightly shorter Pt–Pt edges (2.956 Å) and a longer one (3.074 Å). The second isomer displays C_s symmetry and may be viewed as bent Pt_3 chain with two short Pt–Pt contacts (2.758 Å), whereas the third one is almost non-bonding (3.586 Å). The average values of the Pt–Pt contacts are rather similar in the two isomers (2.995 and 3.034 Å for the C_2 and C_s isomer, respectively), but the variations of individual contacts are rather significant. This point must be carefully considered when evaluating the possibility of this type of isomerism, especially in larger clusters. Indeed, slight variations of the M–M bonding distances are often detected when the same MCC anion has been structurally characterized with different cations, but only in a few cases such variations are sufficiently significant to be called isomers. The same apply when two independent MCCs showing slightly different M–M distances are present within the unit cell of the same crystal structure. Some pertinent examples are represented by $[Rh_{21}Sb_2(CO)_{38}]^{5-}$, $[Rh_{12}Ge(CO)_{27}]^{4-}$ and $[Rh_{12}Sn(CO)_{27}]^{4-}$.[46,90,91]

The case of the two isomers found in the solid state structure of the heteroleptic Chini-type cluster $[Pt_6(CO)_{10}(PPh_3)_2]^{2-}$ is similar to $[Pt_3(\mu\text{-}PPh_2)_3Ph(PPh_3)_2]$.[92] The two isomers have been found in the $[NBu_4]_2[Pt_6(CO)_{10}(PPh_3)_2]$ and $[NBu_4]_2[Pt_6(CO)_{10}(PPh_3)_2]\cdot 2THF$ crystals, respectively (Figure 19). The metal core of both isomers may be described as a distorted octahedron. As usually found in Chini clusters, the intra-triangular Pt–Pt distances are comprised in a very narrow range, that is, 2.66–2.67 Å and 2.66–2.68 Å for the two isomers, respectively. The first isomer shows only two inter-triangular Pt–Pt contacts that may be considered as bonds (3.035 Å), whereas the other four are essentially non-bonding (3.36 and 3.51 Å). Conversely, the second isomer displays four bonding (3.14 and 3.21 Å) and two non-bonding (3.43 Å) inter-triangular Pt–Pt contacts.

Variations of the inter-triangular Pt–Pt contacts may originate, in the solid state, extended isomeric structures in the case of larger homoleptic $[Pt_{3n}(CO)_{6\,n}]^{2-}$ (n = 5–8) Chini clusters.[93–96] Indeed, larger $[Pt_{3n}(CO)_{6\,n}]^{2-}$ (n = 5–8) anions self-assemble during crystallization resulting in infinite pillared chains that, depending on inter-triangular Pt–Pt contacts, may be classified as discontinuous, asymmetric semi-continuous, symmetric semi-continuous, and continuous chains. The molecular identity of each cluster anion is retained within discontinuous chains, since the Pt···Pt contacts between the outer $Pt_3(CO)_6$ units of consecutive cluster anions is slightly greater than the sum of the van der Waals radii. In contrast, continuous chains are based of infinite stacks of $Pt_3(CO)_6$ units displaying similar bonding distances, and the molecular identity of the anions is lost. An intermediate case is represented by semi-continuous chains, that comprise a $Pt_3(CO)_6$ unit shared by two contiguous $[Pt_{3(n-1)}(CO)_{6(n-1)}]^{2-}$ anions with intermediate inter-triangular Pt–Pt distances between continuous and discontinuous. If the shared $Pt_3(CO)_6$ unit is equally located between two $[Pt_{3(n-1)}(CO)_{6(n-1)}]^{2-}$ anions, the chain is named symmetric semi-continuous, whereas the distances are different in asymmetric semi-continuous chains. These different typologies of cluster chains may be viewed as different isomers of the packing of the same Chini anions. For $[Pt_{15}(CO)_{30}]^{2-}$, discontinuous chains have been found in $[NEt_4]_2[Pt_{15}(CO)_{30}]$ and $[Ru(tpy)_2][Pt_{15}(CO)_{30}]\cdot 3DMF$ (tpy = 2,2′:6′,2″-terpyridine), whereas the asymmetric semi-continuous isomer is present within $[Ru(bpy)_3][Pt_{15}(CO)_{30}]\cdot 3CH_3COCH_3$ (bpy = 2,2′-bipyridine). In the case of $[Pt_{18}(CO)_{36}]^{2-}$, the continuous isomer is present within $[Ru(bpy)_2(2\text{-}PTZ)][Pt_{18}(CO)_{36}]$ (2-PTZ = 5-(2-pirydil)tetrazolate) and $[NMe_4]_2[Pt_{18}(CO)_{36}]\cdot 2CH_3COCH_3$, and the symmetric semi-continuous one in $[Ru(bpy)_3][Pt_{18}(CO)_{36}]$ (Figure 20). A further isomer has been found in $[Ph_3P(CH_2)_{12}PPh_3][Pt_{18}(CO)_{36}]$ based on an infinite chain of $[Pt_9(CO)_{18}]^{-}$ anions. Finally, the continuous and symmetric semi-continuous isomers of $[Pt_{24}(CO)_{48}]^{2-}$ are present in $[NEt_4]_2[Pt_{24}(CO)_{48}]$ and $[NBu_4]_2[Pt_{24}(CO)_{48}]$, respectively.

Core Isomerism Involving the Structure of the Metal Kernel

The structure of the metal kernel of MCCs might be a plausible source of isomerism. Nonetheless, the number of such isomers structurally characterized by SC-XRD is very limited. This should be the result of the combination of two factors: (1) synthetic limitations and/or lack of single crystals suitable for SC-XRD; (2) limitations due to the electron counting rules.

To the best of our knowledge, the first example of such isomerism is represented by $[Fe_2Mo_2(\mu_3\text{-}S)_2(\eta^5\text{-}C_5H_5)_2(CO)_6]$.[97] One isomer displays a planar Fe_2Mo_2 core, whereas the second one adopts a butterfly arrangement of the same metal atoms. Including also the two S-atoms, the two isomeric clusters may be described as composed of two $FeMo_2S$ tetrahedra sharing a common Mo–Mo edge. In the planar isomer, the two Fe-atoms are in relative *trans* position, and also the two S-atoms are in *trans.* Conversely, in the butterfly isomer, both Fe and S atoms adopt a relative *cis* arrangement.

More recently, two isomers have been structurally characterized for $[Au_3\{Fe(CO)_4\}_2(PPh_3)_2]^{-}$ as its $[Au(IMes)_2][Au_3\{Fe(CO)_4\}_2(PPh_3)_2]\cdot 0.67CH_2Cl_2$ crystals (IMes = $C_3N_2H_2(C_6H_2Me_3)_2$) (Figure 21).[98] The two isomers are present in a 2:1 ratio within the same crystal structure, and rapidly exchange in solution at all the temperatures, as demonstrated by VT $^{31}P\{^{1}H\}$ NMR spectroscopy. Both isomers are composed of a $[Au_3]^{3+}$ core bonded to

two edge bridging $[Fe(CO)_4]^{2-}$ units and two terminal PPh_3 ligands. In the major isomer, the $[Au_3]^{3+}$ core adopts a V-shaped geometry, whereas it is perfectly linear in the minor isomer. DFT calculations indicate that the energy difference is very small, that is, 0.9 kcal mol^{-1} in favor of the major isomer, in agreement with the fast exchange observed in solution.

An example of structural isomerism involving larger MCCs has been reported for the SC-XRD structures of the two salts $[NEt_4]_4[Ni_{23-x}P_2(CO)_{30-x}]\cdot CH_3COCH_3\cdot$solv (x = 0.82) (**I**) and $[NEt_4]_4[Ni_{22-x}P_2(CO)_{29-x}]\cdot 2CH_3COCH_3$ (x = 0.84) (**II**).[85] As reported in a previous Section, **I** contains a mixture of $[Ni_{23}P_2(CO)_{30}]^{4-}$, $[Ni_{22}P_2(CO)_{29}]^{4-}$ (two isomers), and $[Ni_{21}P_2(CO)_{28}]^{4-}$, because of the presence of two Ni(CO) fragments with partial occupancy factors (0.68 and 0.50). As previously described, the two isomers of $[Ni_{22}P_2(CO)_{29}]^{4-}$ within **I** differ because of the different location of a Ni(CO) fragment on the surface of the cluster. What is relevant to this Section is, in contrast, the comparison of the structures of the $Ni_{18}P_2$ frameworks (Figure 22) contained within **I** and **II**. In **I**, the $Ni_{18}P_2$ framework results from one Ni_9P mono-capped square-antiprism and one $Ni_{10}P$ bicapped square-antiprism sharing a common vertex. The structure is completed by five further Ni atoms not bonded to P, two having partial occupancy factors (0.68 and 0.50). In contrast, the $Ni_{18}P_2$ framework of **II** originated from one Ni_9P mono-capped square-antiprism and one $Ni_{10}P$ distorted sphenocorona and, thus, may be viewed as an isomer of the $Ni_{18}P_2$ framework of **I**. The structure of **II** is completed by four further Ni atom not bonded to P, one with 0.16 occupancy factor. Thus, this salt is composed of $[Ni_{22}P_2(CO)_{29}]^{4-}$ (16%) and $[Ni_{21}P_2(CO)_{28}]^{4-}$ (84%). Overall, **I** and **II** contain core isomers with different metal kernels of both $[Ni_{22}P_2(CO)_{29}]^{4-}$ and $[Ni_{21}P_2(CO)_{28}]^{4-}$. Moreover, **I** contains also two surface isomers of $[Ni_{22}P_2(CO)_{29}]^{4-}$ differing for the location of one Ni(CO) fragment.

The most impressive example of core isomerism in MCCs is represented by $[HCo_{15}Pd_9C_3(CO)_{38}]^{2-}$, which belongs to the $[H_{3-n}Co_{15}Pd_9C_3(CO)_{38}]^{n-}$ (n = 0–3) family of clusters.[99,100] The species $[HCo_{15}Pd_9C_3(CO)_{38}]^{2-}$ is obtained in good yields in a two steps synthesis. First, $[Co_6C(CO)_{15}]^{2-}$ is reacted with $Pd(Et_2S)_2Cl_2$ affording $[H_2Co_{20}Pd_{16}C_4(CO)_{48}]^{4-}$. This, in turn, is converted into $[HCo_{15}Pd_9C_3(CO)_{38}]^{2-}$ upon reaction with a slight excess of $HBF_4\cdot Et_2O$ in CH_2Cl_2 (Scheme 4). The dianion $[HCo_{15}Pd_9C_3(CO)_{38}]^{2-}$ is further protonated with $HBF_4\cdot Et_2O$ resulting in $[H_2Co_{15}Pd_9C_3(CO)_{38}]^{-}$ and, eventually, $[H_3Co_{15}Pd_9C_3(CO)_{38}]$. Deprotonation with a strong base such as NaOH leads to $[Co_{15}Pd_9C_3(CO)_{38}]^{3-}$.

The species $[H_{3-n}Co_{15}Pd_9C_3(CO)_{38}]^{n-}$ (n = 0–3) are all composed of a $Pd_9(\mu_3\text{-}CO)_2$ core decorated on the surface by three square-pyramidal $Co_5C(CO)_{12}$ fragments. The $Pd_9(\mu_3\text{-}CO)_2$ core adopts a tri-capped octahedral structure (Oh-Pd_9) in $[H_3Co_{15}Pd_9C_3(CO)_{38}]$ and $[H_2Co_{15}Pd_9C_3(CO)_{38}]^{-}$, whereas a tri-capped trigonal prism (TP-Pd_9) is present in $[Co_{15}Pd_9C_3(CO)_{38}]^{3-}$. In the case of $[HCo_{15}Pd_9C_3(CO)_{38}]^{2-}$, both Oh-$Pd_9$ and TP-Pd_9 core isomers have been isolated and structurally characterized (Figures 23 and 24). Which isomer is present in the solid state depends on the cation employed and/or the number and type of co-crystallized solvent molecules. Moreover, mixtures of the Oh-Pd_9 and TP-Pd_9 isomers of $[HCo_{15}Pd_9C_3(CO)_{38}]^{2-}$ are often found within the same crystal, or even mixtures of crystals containing different isomers are found within the same crystallization batch. This is probably the first example of cluster core isomerism induced by crystal packing effects reported for molecular nanoclusters. It is noteworthy that, in this case, weak intermolecular packing forces strongly affect the structure of the cluster core, and are not limited to surface ligands or fragments as described in the previous Sections. It must be remarked, also, that the $[H_{3-n}Co_{15}Pd_9C_3(CO)_{38}]^{n-}$ (n = 0–3) clusters are reversibly interconverted by simple acid-base reactions. All these results suggest that sometimes the core of even larger clusters is rather soft and can be easily transformed by protonation/deprotonation processes or even packing forces during crystallization.

Core Isomerism Involving the Position of Metal Atoms Within the Metal Kernel

In the case of heterometallic MCCs, two clusters may have the same structure of the metal core and the same (or very similar) stereochemistry of the ligands, but a different disposition of the metal atoms within the metal kernel. This kind of isomerism has been documented for the *cis* and *trans* isomers of the boride clusters $[Rh_2Fe_4B(CO)_{16}]^{-}$ (Scheme 5), $[Rh_2Ru_4B(CO)_{16}]^{-}$ and $[Rh_2Ru_4B(CO)_{16}(AuPPh_3)]$.[101–104] For the latter cluster, ^{11}B NMR studies demonstrated that, on standing in solution, *cis* converted to *trans*.[105] In this case, *cis* and *trans* refer to the disposition of the two Rh and four Fe or Ru atoms within the octahedral core of the clusters.

Generally speaking, the different metal atom types of heterometallic MCCs may be perfectly ordered, randomly distributed, or may display a partial site preference, which

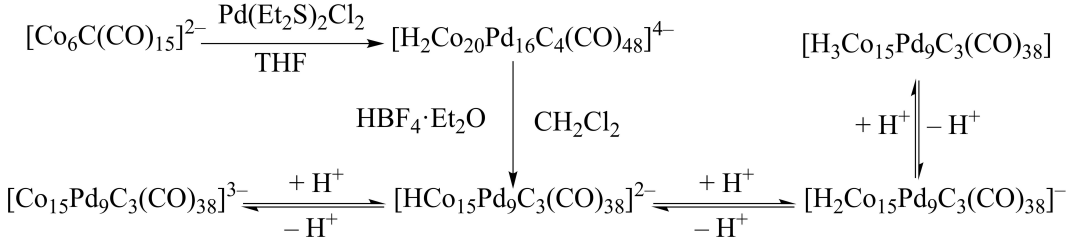

Scheme 4. Synthesis of $[H_{3-n}Co_{15}Pd_9C_3(CO)_{38}]^{n-}$ (n = 0–3). Protons are added with strong acids, such as $HBF_4\cdot Et_2O$, and removed with strong bases, such as NaOH.

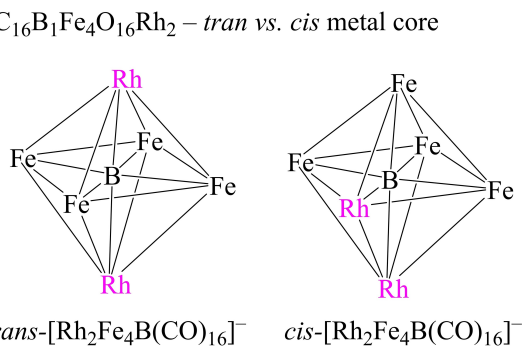

Scheme 5. Core isomerism – Different position of Fe and Rh atoms within the metal kernel. $[Rh_2Fe_4B(CO)_{16}]^-$ exists as *trans* and *cis* isomers due to the different locations of Fe and Rh atoms within the octahedral metal core. CO ligands have been omitted.

means also partial disorder.[106–109] Perfectly ordered structures originate when the different metal types occupy precise positions within the metal polyhedron. If this is strictly followed, one structure is far more stable than all other positional isomers, originating a single structure with all metal types located in unique sites. A slight relaxation of this site selectivity may lower the energy difference among structures with different metal locations, leading to isomers involving the position of the metals within the metal kernel. This point is well exemplified by the above mentioned Rh_2Fe_4B and Rh_2Ru_4B clusters. In particular, in the case of $[Rh_2Ru_4B(CO)_{16}(AuPPh_3)]$, the *cis* isomer may be viewed as the kinetic isomer and the *trans* one as the thermodynamic isomer.

Two isomers are formed in the case of $[Ni_{10}Rh_2C(CO)_{20}]^{2-}$, but these cannot be separated and, thus, they are always obtained in mixture, both in solution and in the solid state as indicated by ^{13}C NMR spectroscopy and SC-XRD (Figure 25).[110] These two isomers differ for the location of the two Rh atoms on the two outer edges of the $Ni_{10}Rh_2$ tetra-capped bis-disphenoid cage. The two isomers co-crystallize generating partial Ni/Rh disorder on these four metal sites. ^{13}C NMR studies indicate that the isomer ratio in solution is 4:1, with very similar spectroscopic features (major isomer, triplet, $\delta_P = 362.9$ ppm, $^1J_{C\text{-}Rh} = 11.5$ Hz, $T_1 = 6.5 \pm 0.3$ s; minor isomer, triplet, $\delta_P = 363.7$ ppm, $^1J_{C\text{-}Rh} = 9.1$ Hz, $T_1 = 6.3 \pm 0.5$ s). The two isomers of $[Ni_{10}Rh_2C(CO)_{20}]^{2-}$ have been obtained from the reaction of $[Ni_9C(CO)_{17}]^{2-}$ with $[Rh(COD)Cl]_2$, in mixture with $[Ni_9Rh_3C(CO)_{20}]^{3-}$ (quartet, $\delta_P = 378.3$ ppm, $^1J_{C\text{-}Rh} = 9.6$ Hz, $T_1 = 3.4 \pm 0.6$ s), which can be separated owing their different solubilities in organic solvents. The three Rh atoms of $[Ni_9Rh_3C(CO)_{20}]^{3-}$ are randomly distributed over the same four metal sites as in the isostructural $[Ni_{10}Rh_2C(CO)_{20}]^{2-}$. This further supports the fact that these four sites can be similarly occupied by Ni and Rh.

Further relaxing site preference leads to local disorder of the site occupation and, eventually, to the random distribution of the different metals over all the sites of the metal kernel. Randomization of the metal site occupation has been observed for $[Co_3Ni_9C(CO)_{20}]^{n-}$,[111] and $[Fe_xRh_{6-x}(CO)_{20}]^{x-}$,[112] whereas partial metal disorder has been documented for $[Pt_6Ru_6(CO)_{28}]^{2-}$.[113]

Complete randomization of the metal sites leads to molecular random alloy clusters, as found in heterometallic Ni–Pt Chini-type MCCs such as $[Pt_{6-x}Ni_x(CO)_{12}]^{2-}$ (x = 1–5).[114] Mixtures of these clusters, whose compositions may be varied in an almost continuous way, may be obtained just by mixing $[Pt_6(CO)_{12}]^{2-}$ and $[Ni_6(CO)_{12}]^{2-}$ in different stoichiometric ratios. A combination of IR, ^{195}Pt and ^{13}C NMR spectroscopy, ESI-MS, MP-AES, SC-XRD and DFT studies indicate that each sample is actually a mixture of different $[Pt_{6-x}Ni_x(CO)_{12}]^{2-}$ (x = 0–6) species, whose average composition depends on the stoichiometry of the reagents. Moreover, three isomers are present for $[Pt_4Ni_2(CO)_{12}]^{2-}$, $[Pt_3Ni_3(CO)_{12}]^{2-}$, and $[Pt_2Ni_4(CO)_{12}]^{2-}$, which differ for the Ni/Pt distribution over the six equivalent positions of the octahedral metal cage (Figure 26).

When different metal sites are present, Pt usually prefers those with high M–M and low M–CO connectivity, and the opposite applies to Ni. This may lead to complete metal segregation, as found in $[H_{3-n}Ni_{38}Pt_6(CO)_{44}]^{n-}$ (n = 3–6),[115,116] or partial metal segregation, often accompanied by Ni/Pt substitutional disorder, some representative examples being $[Ni_{35}Pt_9(CO)_{44}]^{6-}$, $[Ni_{32}Pt_{24}(CO)_{56}]^{6-}$, $[Pt_{12-x}Ni_x(CO)_{21}]^{4-}$ (x = 2–10), $[Pt_{19-x}Ni_x(CO)_{22}]^{4-}$ (x = 2–6), $[HPt_{14+x}Ni_{24-x}(CO)_{44}]^{5-}$ (x = 0, 1) (Figure 27).[117–119] Partial substitutional disorder has been established also for several heterometallic Ni–Pd MCCs.[106,107] Indeed, the SC-XRD structures of several Ni–Pd MCCs display some metal sites with Ni/Pd substitutional disorder, that could indicate also the presence of mixtures of positional isomers.

Substitutional and composition disorder is present also in the 2-D molecular alloy clusters $[M_xM'_{5-x}Fe_4(CO)_{16}]^{3-}$ (M, M′ = Cu, Ag, Au; M ≠ M′; x = 0–5).[120] Their structures are based on a centred $M_xM'_{5-x}$ rectangle, displaying a unique central position and four equivalent corner positions (Figure 28). All coinage metals can occupy these different positions, even though some site preference is present. Overall, as in the case of $[Pt_{6-x}Ni_x(CO)_{12}]^{2-}$ (x = 0–6), mixtures of clusters with different values of x as well as positional isomers are always present in solution and in the solid state.

To conclude this Section, the two clusters $[W_2RhIr_2(\mu\text{-}CO)_3(CO)_6(\eta^5\text{-}C_5H_5)_2(\eta^5\text{-}C_5HMe_4)]$ and $[W_2RhIr_2(\mu\text{-}CO)_4(CO)_5(\eta^5\text{-}C_5H_5)_2(\eta^5\text{-}C_5HMe_4)]$ have been described as a case of dynamic permutational isomerism (Figure 29).[121] These trigonal bypiramidal clusters differ because in the former the equatorial positions are occupied by two Ir and one W atom, whereas in the latter the equatorial positions consist of one Ir and two W atoms. From this point of view, these are core isomers that differ for the positions of the metal atom types within the same polyhedron. Nonetheless, also the location of the ligands is different. Indeed, $[W_2RhIr_2(\mu\text{-}CO)_3(CO)_6(\eta^5\text{-}C_5H_5)_2(\eta^5\text{-}C_5HMe_4)]$ displays only one C_5H_5 ligand (bonded to W) in the equatorial plane, whereas the other C_5H_5 ligand (bonded to W) and C_5HMe_4 (bonded to Rh) are in apical positions. Conversely, in $[W_2RhIr_2(\mu\text{-}CO)_4(CO)_5(\eta^5\text{-}C_5H_5)_2(\eta^5\text{-}C_5HMe_4)]$, both C_5H_5 ligands (bonded to W) are in the equatorial plane, whereas C_5HMe_4 (bonded to Rh) is in apical position. From this point of view, these clusters may be described as isomers that differ for the location of ML fragments. Moreover, also the stereochemistry of the CO ligands is slightly different. Overall, this may be

described as a case of complex isomerism, resulting from the combination of different typologies of isomerism. The permutational isomers slowly interconvert in solution by a cluster metal vertex exchange that is proposed to proceed by Rh–Ir and Rh–W bond cleavage and reformation, and via the intermediacy of an edge-bridged tetrahedral transition state. The permutational isomers display differing chemical and physical properties: replacement of CO by PPh_3 occurs at one permutational isomer only, while the isomers display distinct optical power limiting behaviour.

Polymerisation and Coordination Isomerism

Polymerization isomers may be defined as two compounds having the same elemental compositions and ligand distribution, but different molecular weights. In the case of coordination isomerism, the two compounds have the same elemental compositions, but different molecular weights and different ligand distribution. Both polymerization and coordination isomerism are rather rare in MCC chemistry.

To the best of our knowledge, coordination isomerism has been documented only for the carbonyl compounds (IMes)Cu-[M] and $\{(IMes)_2Cu\}\{Cu[M]_2\}$ ([M] = Mc, $Mn(CO)_5^-$; Cc, $Co(CO)_4^-$; Mp, $MoCp(CO)_3^-$; Crp, $CrCp(CO)_3^-$), which establish an equilibrium in solution. Only in the case of (IMes)Cu–Mc and $\{(IMes)_2Cu\}\{CuMc_2\}$, both isomers have been structurally characterized by SC-XRD (Scheme 6).[122]

Polymerization isomerism has been demonstrated for $[\{MFe(CO)_4\}_3]^{3-}$ and $[\{MFe(CO)_4\}_4]^{4-}$ (M = Ag, Au), which may be described as trimers and tetramers of $[\{MFe(CO)_4\}]^-$, respectively (Figure 30).[123] Similarly, $[Ag\{Co(CO)_4\}_2]^-$ and $[Ag_2\{Co(CO)_4\}_4]^{2-}$ are the monomer and dimer, respectively, of the same molecular unit (Figure 31).[45]

A further example of polymerization isomerism is represented by the Ru tetracarbonyl, that may exist as a $[Ru_3(CO)_{12}]$ trimer or an infinite $[Ru(CO)_4]_\infty$ polymer.[124] Moreover, the 1:1 adduct between Cu^+ and $[Co(CO)_4]^-$ may originate a $[CuCo(CO)_4]_4$ tetramer or an infinite $[CuCo(CO)_4]_\infty$ polymer (Figure 32).[125,126]

All the above mentioned examples of polymerization isomerism are based on M–M bonds, whereas the square tetramer $[Fe_4Cu_2(\mu_6\text{-}C)(CO)_{12}(bipy)]_4$ (bipy = 4,4′-bipyridine) and the infinite zig-zag chain polymer $[Fe_4Cu_2(\mu_6\text{-}C)(CO)_{12}(bipy)]_\infty$ are polymerization isomers generated by the bridging ligands (Figure 33).[127]

Conclusions

Several examples of isomerism have been reported along the years for molecular MCCs of different sizes. These include surface isomerism as well as core isomerism. Surface isomers may originate from the stereochemistry of the carbonyl ligands in the case of homoleptic MCCs. The presence of other inorganic (often hydrides) or organic ligands introduces further potential sources of isomerism, that is, coordination site (position), coordination mode, reciprocal disposition of the ligands, overall 3-D arrangement of the ligand shell. Moreover, the metal core of the cluster may be decorated on the surface by miscellaneous ML fragments, whose geometrical disposition may generate further surface isomers. The latter phenomenon

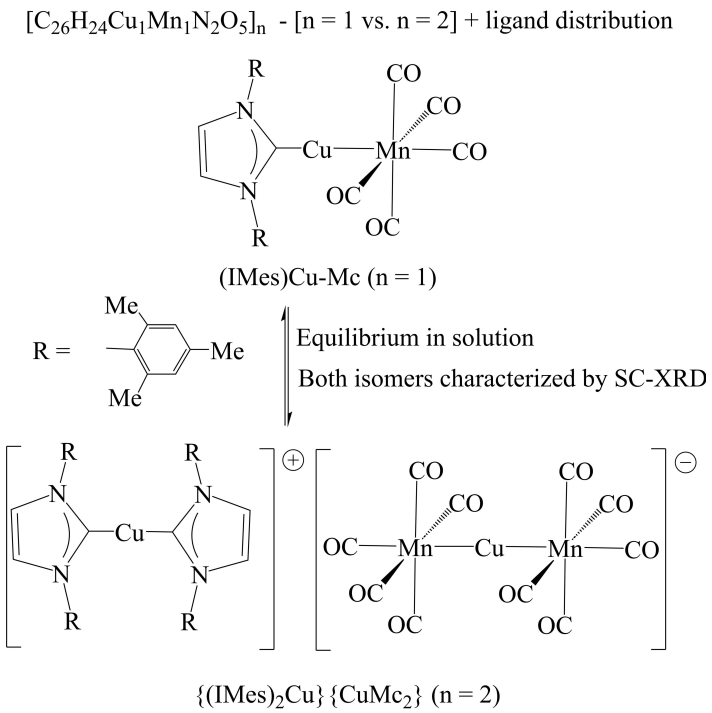

Scheme 6. Coordination isomerism – Schematic representation of the two isomers (IMes)Cu–Mc and $\{(IMes)_2Cu\}\{CuMc_2\}$. The isomers are in equilibrium in solution, and they have been both structurally characterized in the solid state by SC-XRD.

is closely related to isomerism due to the staple motives in ligand protected coinage metal molecular nanoclusters.[1–17] It must be remarked that often MCCs, in the solid state, occupy general positions lacking site symmetry, and this may result in chiral MCCs. Nonetheless, the presence of inversion centres, mirror or glide planes in the space group generates a racemic mixture within the crystal. Therefore, genuine cases of enantiomerism in MCC have not been yet demonstrated, unless a chiral ligand is introduced.[128,129]

Core isomerism in MCCs may concern significant variations of M–M contacts among different isomers without any further relevant difference, as well as changes of the structures of the metal core (polyhedron) of the MCC. In the latter case, the Oh-Pd_9 and TP-Pd_9 isomers of $[HCo_{15}Pd_9C_3(CO)_{38}]^{2-}$ represent one of the most significant example for high nuclearity MCCs. The reversible interconversion of the Oh-Pd_9 and TP-Pd_9 cores upon protonation/deprotonation of the related clusters $[H_{3ss-n}Co_{15}Pd_9C_3(CO)_{38}]^{n-}$ (n = 0–3), as well as isomerization of $[HCo_{15}Pd_9C_3(CO)_{38}]^{2-}$ upon crystallization, indicate that the core of even larger clusters may be transformed by weak forces. This might be taken into consideration when analyzing catalysis by ultra-small metal nanoparticles and molecular nanoclusters.[130–132]

Positional isomers are possible for heterometallic MCCs in view of the fact that the same metal site (position) may be occupied by different metal types. Separation of such isomers is not very straightforward and, often, this results in mixtures of two or more positional isomers in solution and in the solid state. Within a single crystal, the co-crystallization of positional isomers generates positional disorder, that makes sometimes rather difficult the identification of the actual isomers. A further complication arises since, often, positional disorder is accompanied by substitutional disorder. Indeed, both these phenomena are caused by a limited metal site selectivity, which is more likely in the case of isoelectronic metal couples, such as, Ni/Pt, Ni/Pd, Cu/Ag, Cu/Au, Ag/Au. The combination of positional and substitutional disorder generates mixtures of isostructural MCCs with different ratios of the two metal types as well as mixtures of positional isomers. Shedding light into these complex mixtures of MCCs is a real challenge that might help a better understanding of molecular alloy nanoclusters.

As a concluding remark, the study of isomerism in MCCs of increasing sizes, and the identification of different types of isomerism, including rare typologies such as polymerization and coordination isomerism, represent a challenge for the future. Surface and core isomerism are found in all classes of molecular nanoclusters and, thus, their systematic study is fundamental for the development of nanochemistry, the understanding of its mechanisms, and the applications of ultra-small metal nanoparticles and nanoclusters.

Acknowledgements

Financed by the European Union - NextGenerationEU through the Italian Ministry of University and Research under PNRR - Mission 4 Component 1, Investment 4.1 (DM 118/2023)CUP J33C23002200002. Open Access publishing facilitated by Università degli Studi di Bologna, as part of the Wiley - CRUI-CARE agreement.

Conflict of Interests

The authors declare no conflict of interest.

Keywords: Metal cluster · Isomerism · Carbonyl ligand · Molecular nanocluster · Crystal structure

[1] X. Kang, M. Zhu, *Chem. Mater.* **2021**, *33*, 39–62.
[2] T. Higaki, Y. Li, S. Zhao, Q. Li, S. Li, X.-S. Du, S. Yang, J. Chai, R. Jin, *Angew. Chem. Int.* **2019**, *58*, 8291–8302.
[3] L. He, X. He, J. Wang, Y. Qu, X. Su, J. Zheng, X. Zhao, *CrystEngComm.* **2020**, *22*, 6975–6978.
[4] W. W. Xu, X. C. Zeng, Y. Gao, *Nanoscale* **2018**, *10*, 9476–9483.
[5] W. W. Xu, X. C. Zeng, Y. Gao, *Acc. Chem. Res.* **2018**, *51*, 2739–2747.
[6] S. Tian, Y.-Z. Li, M.-B. Li, J. Yuan, J. Wang, Z. Wu, R. Jin, *Nat. Commun.* **2015**, *6*, 8667.
[7] R. Jin, C. Zeng, M. Zhou, Y. Chen, *Chem. Rev.* **2016**, *116*, 10346–10413.
[8] X. Kang, Y. Li, M. Zhu, R. Jin, *Chem. Rev.* **2020**, *49*, 6443–6514.
[9] D. M. P. Mingos, in *50th Anniversary of Electron Counting Paradigms for Polyhedral Molecules. Structure and Bonding.* (Eds: D. M. P. Mingos), vol. 188, Springer, **2021**.
[10] Y. Cao, S. Malola, M. F. Matus, T. Chen, Q. Yao, R. Shi, H. Häkkinen, J. Xie, *Chem* **2021**, *7*, 227–2244.
[11] G. U. Kuda-Singappulige, P. S. Window, C. A. Hosier, I. D. Anderson, C. M. Aikens, C. J. Ackerson, *Chem. Eur. J.* **2024**, *30*, e202202760.
[12] Y.-R. Ni, M. N. Pillay, T.-H. Chiu, Y.-Y. Wu, S. Kahlal, J.-Y. Saillard, C. W. Liu, *Chem. Eur. J.* **2023**, *29*, e202300730.
[13] Y. Chen, C. Liu, Q. Tang, C. Zeng, T. Higaki, A. Das, D. Jiang, N. L. Rosi, R. Jin, *J. Am, Chem. Soc.* **2016**, *138*, 1482–1485.
[14] Q. Li, Y. Tan, B. Huang, S. Yang, J. Chai, X. Wang, Y. Pei, M. Zhu, *J. Am. Chem. Soc.* **2023**, *145*, 15859–15868.
[15] Z. Qin, J. Zhang, C. Wan, S. Liu, H. Abroshan, R. Jin, G. Li, *Nat. Commun.* **2020**, *11*, 6019.
[16] Y. Fujiki, T. Matsuyama, S. Kikkawa, J. Hirayama, H. Takaya, N. Nakatani, N. Yasuda, K. Nitta, Y. Negishi, S. Yamazoe, *Commun. Chem.* **2023**, *6*, 129.
[17] S. Biswas, S. Das, Y. Negishi, *Nanoscale Horiz.* **2023**, *8*, 1509–1522.
[18] A. V. Virovets, E. Peresypkina, M. Scheer, *Chem. Rev.* **2021**, *121*, 14485–14554.
[19] J. E. McGrady, F. Weigend, S. Dehnen, *Chem. Soc. Rev.* **2022**, *51*, 628–649.
[20] R. Bender, P. Braunstein, A. Tiripicchio, M. Tiripicchio-Camellini, *Angew. Chem. Int. Ed.* **1985**, *24*, 861–862.
[21] R. Bender, P. Braunstein, A. Dedieu, P. D. Ellis, B. Huggins, P. D. Harvey, E. Sappa, A. Tiripicchio, *Inorg. Chem.* **1996**, *35*, 1223–1234.
[22] R. Bender, R. Welter, P. Braunstein, *Inorg. Chim. Acta* **2015**, *424*, 20–28.
[23] G. Schmid (Ed.), *Clusters and Colloids*, Wiley-VCH, New York, **1994**.
[24] P. Braunstein, L. A. Oro, P. R. Raithby (Eds.), *Metal Clusters in Chemistry*, Wiley-VCH, New York, **1999**.
[25] S. Zacchini, *Eur. J. Inorg. Chem.* **2011**, *2011*, 4125–4145.
[26] C. Femoni, F. Kaswalder, M. C. Iapalucci, G. Longoni, S. Zacchini, *Coord. Chem. Rev.* **2006**, *250*, 1580–1604.
[27] B. Berti, C. Femoni, M. C. Iapalucci, S. Ruggieri, S. Zacchini, *Eur. J. Inorg. Chem.* **2018**, *2018*, 3285–3296.
[28] E. G. Mednikov, L. F. Dahl, *Soc. A* **2010**, *368*, 1301–1322.
[29] G. Hogarth, S. E. Kabir, E. Nordlander, *Dalton Trans.* **2010**, *39*, 6153–6174.
[30] P. R. Raithby, *J. Organomet, Chem.* **2024**, *1005*, 122979.
[31] C. Cesari, J.-H. Shon, S. Zacchini, L. A. Berben, *Chem. Soc. Rev.* **2021**, *50*, 9503–9539.
[32] K. L. Kollmannsberger, C. Poonam, *Chem. Mater.* **2023**, *35*, 5475–5486.
[33] P. M. Schneider, K. L. Kollmannsberger, C. Cesari, R. Khare, M. Boniface, B. R. Cuenya, T. Lunkenbein, M. Elsner, S. Zacchini, A. S. Bandarenka, J. Warnan, R. A. Fischer, *ChemElectroChem* **2024**, *11*, e202300476.

[34] S. Pattanayak, N. D. Loewen, L. A. Berben, *Inorg. Chem.* **2023**, *62*, 1919–1925.
[35] 'isomer' in *IUPAC Compendium of Chemical Terminology*, 3rd ed. International Union of Pure and Applied Chemistry; 2006. Online version 3.0.1, 2019. 10.1351/goldbook.I03289.
[36] B. F. G. Johnson, E. A. Quadrelli, V. Ferrand, A. W. Bott, *J. Chem. Soc. Dalton Trans.* **2001**, 1063–1068.
[37] T. Y. Garcia, J. C. Fettinger, M. M. Olmstead, A. L. Balch, *Chem. Commun.* **2009**, 7143–7145.
[38] E. F. Paulus, *Acta Crystal.* **1969**, *B25*, 2206–2213.
[39] L. Garlaschelli, M. Martinengo, P. L. Bellon, F. Demartin, M. Manassero, M. Y. Chiang, C. Wei, R. Bau, J . *Am, Chem. Soc.* **1984**, *106*, 6664–6667.
[40] G. Manca, F. Fabrizi de Biani, M. Corsini, C. Cesari, C. Femoni, M. C. Iapalucci, S. Zacchini, A. Ienco, *Inorg. Chem.* **2022**, *61*, 3484–3492.
[41] C. Femoni, M. C. Iapalucci, G. Longoni, C. Tiozzo, J. Wolowska, S. Zacchini, E. Zazzaroni, *Chem. Eur. J.* **2007**, *13*, 6544–6554.
[42] G. Süss-Fink, S. Haak, V. Ferrand, H. Stoeckli-Evans, *J. Chem. Soc., Dalton Trans.* **1997**, 3861–3866.
[43] A. Fumagalli, M. C. Malatesta, M. Vallario, G. Ciani, M. Moret, A. Sironi, *J. Clust, Sci.* **2001**, *12*, 187–200.
[44] C. E. Plečnik, S. Liu, X. Chen, E. A. Meyers, S. G. Shore, *J. Am, Chem. Soc.* **2004**, *126*, 204–213.
[45] C. Cesari, B. Berti, F. Calcagno, C. Femoni, M. Garavelli, M. C. Iapalucci, I. Rivalta, S. Zacchini, *Molecules* **2021**, *26*, 1529.
[46] F. L. Bowles, M. M. Olmstead, C. M. Beavers, A. L. Balch, *Chem. Commun.* **2013**, *49*, 5921–5923.
[47] C. Femoni, M. C. Iapalucci, G. Longoni, C. Tiozzo, S. Zacchini, B. T. Heaton, J. A. Iggo, *Dalton Trans.* **2007**, 3914–3923.
[48] A. Fumagalli, S. Martinengo, G. Ciani, A. Sironi, B. T. Heaton, *J. Chem. Soc. Dalton Trans.* **1988**, 163–171.
[49] M. McPartlin, W. J. H. Nelson, *J. Chem. Soc. Dalton Trans.* **1986**, 1557–1563.
[50] K. E. Inkrott, S. G. Shore, *Inorg. Chem.* **1979**, *18*, 2817–2821.
[51] C. Cesari, M. Bortoluzzi, C. Femoni, M. C. Iapalucci, S. Zacchini, *Dalton Trans.* **2021**, *50*, 9610–9622.
[52] J. A. Cabeza, P. Garciá-Álvarez, *Chem. Soc. Rev.* **2011**, *40*, 5389–5405.
[53] V. H. Hansen, A. K. Ma, K. Biradha, R. K. Pomeroy, M. J. Zaworotko, *Organometallics* **1998**, *17*, 5267–5274.
[54] S. P. Tunik, A. V. Vlasov, K. V. Kogdov, G. L. Starova, A. B. Nikol'skii, *J. Organomet, Chem.* **1994**, *479*, 59–72.
[55] D. Belletti, C. Graiff, R. Pattacini, G. Predieri, A. Tiripicchio, F. Fabrizi de Biani, P. Zanello, *Inorg. Chim. Acta* **2005**, *358*, 161–172.
[56] W. G.-Y. Ho, W.-T. Wong, *Polyhedron* **1995**, *14*, 2849–2855.
[57] C. Cesari, I. Ciabatti, C. Femoni, M. C. Iapalucci, F. Mancini, S. Zacchini, *Inorg. Chem.* **2017**, *56*, 1655–1668.
[58] N. A. Pusharevsky, S. N. Konchenko, M. Scheer, *J. Clust. Sci.* **2007**, *18*, 606–617.
[59] R. D. Adams, J. Kiprotich, D. V. Peryshkov, Y. O. Wong, *Chem. Eur. J.* **2016**, *22*, 6501–6504.
[60] P. R. Raithby, G. P. Shields, *Polyhedron* **1998**, *17*, 2829–2856.
[61] D. Braga, P. J. Dyson, F. Grepioni, B. F. G. Johnson, *Chem. Rev.* **1994**, *94*, 1585–1620.
[62] D. B. Brown, P. J. Dyson, B. F. G. Johnson, D. Parker, *J. Organomet, Chem.* **1995**, *491*, 189–193.
[63] R. D. Adams, V. Rassolov, Q. Zhang, *Organometallics* **2013**, *32*, 6368–6378.
[64] R. D. Adams, M. Kaushal, M. D. Smith, N. D. Wakdikar, *J. Organomet. Chem.* **2022**, *982*, 122538.
[65] M. W. Lum, W. K. Leong, *J. Organomet. Chem.* **2003**, *687*, 203–208.
[66] S. A. Begum, A. H. Chowdhury, S. Ghosh, D. A. Tocher, E. Rosemberg, K. I. Hardcastle, S. E. Kabir, *Inorg. Chim. Acta* **2018**, *478*, 25–31.
[67] J. Fu, G. J. Moxey, M. Morshedi, A. Barlow, M. D. Randles, P. V. Simpson, T. Schwich, M. P. Cifuentes, M. G. Humphrey, *J. Organomet. Chem.* **2016**, *812*, 135–144.
[68] A. V. Virovets, S. N. Konchenko, P. S. Yuferov, D. Fenske, *J. Struct. Chem.* **2004**, *45*, 496–501.
[69] H. Wadepohl, S. Gebert, H. Pritzkow, F. Grepioni, D. Braga, *Chem. Eur. J.* **1998**, *4*, 279–288.
[70] H.-J. Kneuper, J. R. Shapley, *Organometallics* **1987**, *6*, 2455–2456.
[71] J. S.-Y. Wong, W.-T. Wong, *New J. Chem.* **2002**, *26*, 94–104.
[72] C. Cesari, C. Femoni, M. C. Iapalucci, S. Zacchini, *Inorg. Chim. Acta* **2023**, *544*, 121235.
[73] I. Ciabatti, C. Femoni, M. C. Iapalucci, G. Longoni, S. Zacchini, *J. Clust. Sci.* **2014**, *25*, 115–146.
[74] M. Bortoluzzi, A. Ceriotti, I. Ciabatti, R. Della Pergola, C. Femoni, M. C. Iapalucci, A. Storione, S. Zacchini, *Dalton Trans.* **2016**, *45*, 5001–5013.
[75] I. Ciabatti, C. Femoni, M. C. Iapalucci, S. Ruggieri, S. Zacchini, *Coord. Chem. Rev.* **2018**, *355*, 27–38.
[76] P. Braunstein, J. Rose, *Gold Bull.* **1985**, *18*, 17–30.
[77] Z. Akhter, J. F. Gallagher, J. Lewis, P. R. Raithby, G. P. Shields, *J. Organomet. Chem.* **2000**, *614–615*, 231–237.
[78] I. Ciabatti, C. Femoni, M. Hayatifar, M. C. Iapalucci, A. Ienco, G. Longoni, G. Manca, S. Zacchini, *Inorg. Chem.* **2014**, *53*, 9761–9770.
[79] I. Ciabatti, C. Femoni, M. Hayatifar, M. C. Iapalucci, S. Zacchini, *Inorg. Chim. Acta* **2015**, *428*, 203–211.
[80] I. Ciabatti, C. Femoni, M. C. Iapalucci, A. Ienco, G. Longoni, G. Manca, S. Zacchini, *Inorg. Chem.* **2013**, *52*, 10559–10565.
[81] C. Cesari, M. Bortoluzzi, C. Femoni, F. Forti, M. C. Iapalucci, S. Zacchini, *Dalton Trans.* **2024**, *53*, 3865–3879.
[82] D. M. P. Mingos, D. J. Wales, *Introduction to Cluster Chemistry*, Prentice Hall, Englewood Cliffs **1990**.
[83] C. Cesari, I. Ciabatti, C. Femoni, M. C. Iapalucci, S. Zacchini, *J. Clust. Sci.* **2017**, *28*, 1963–1979.
[84] C. Femoni, M. C. Iapalucci, G. Longoni, S. Zacchini, S. Fedi, F. Fabrizi de Biani, *Dalton Trans.* **2012**, *41*, 4649–4663.
[85] C. Capacci, C. Cesari, C. Femoni, M. C. Iapalucci, F. Mancini, S. Ruggieri, S. Zacchini, *Inorg. Chem.* **2020**, *59*, 16016–16026.
[86] R. D. Adams, B. Captain, W. Fu, P. J. Pellechia, M. D. Smith, *Inorg. Chem.* **2003**, *42*, 2094–2101.
[87] R. D. Adams, B. Captain, W. Fu, M. D. Smith, *J. Am. Chem. Soc.* **2002**, *124*, 5628–5629.
[88] M. Shieh, C.-Y. Miu, K.-J. Hsing, L.-F. Jang, C.-N. Lin, *Dalton Trans.* **2015**, *44*, 6526–6536.
[89] D. Collini, F. Fabrizi de Biani, S. Fedi, C. Femoni, F. Kaswalder, M. C. Iapalucci, G. Longoni, C. Tiozzo, S. Zacchini, P. Zanello, *Inorg. Chem.* **2007**, *46*, 7971–7981.
[90] C. Femoni, T. Funaioli, M. C. Iapalucci, S. Ruggieri, S. Zacchini, *Inorg. Chem.* **2020**, *59*, 4300–4310.
[91] A. Boccalini, P. J. Dyson, C. Femoni, M. C. Iapalucci, S. Ruggieri, S. Zacchini, *Dalton Trans.* **2018**, *47*, 15737–15744.
[92] I. Ciabatti, C. Femoni, M. C. Iapalucci, G. Longoni, T. Lovato, S. Zacchini, *Inorg. Chem.* **2013**, *52*, 4384–4395.
[93] C. Femoni, M. C. Iapalucci, G. Longoni, T. Lovato, S. Stagni, S. Zacchini, *Inorg. Chem.* **2010**, *49*, 5992–6004.
[94] C. Femoni, F. Kaswalder, M. C. Iapalucci, G. Longoni, S. Zacchini, *Eur. J. Inorg. Chem.* **2007**, *1*, 483–1486.
[95] C. Femoni, F. Kaswalder, M. C. Iapalucci, G. Longoni, M. Mehlstäubl, S. Zacchini, A. Ceriotti, *Angew. Chem. Int. Ed.* **2006**, *45*, 2060–2062.
[96] B. Berti, M. Bortoluzzi, A. Ceriotti, C. Cesari, C. Femoni, M. C. Iapalucci, S. Zacchini, *Inorg. Chim. Acta* **2020**, *512*, 119904.
[97] T. P. Fehlner, C. E. Housecroft, K. Wade, *Organometallics* **1983**, *2*, 1426–1428.
[98] B. Berti, M. Bortoluzzi, C. Cesari, C. Femoni, M. C. Iapalucci, R. Mazzoni, F. Vacca, S. Zacchini, *Inorg. Chem.* **2020**, *59*, 2228–2240.
[99] B. Berti, I. Ciabatti, C. Femoni, M. C. Iapalucci, S. Zacchini, *ACS Omega* **2018**, *3*, 13239–13250.
[100] I. Ciabatti, C. Femoni, M. Gaboardi, M. C. Iapalucci, G. Longoni, D. Pontiroli, M. Riccò, S. Zacchini, *Dalton Trans.* **2014**, *43*, 4388–4399.
[101] R. Khattar, J. Puga, T. P. Fehlner, A. L. Rheingold, *J. Am, Chem. Soc.* **1989**, *111*, 1877–1879.
[102] A. K. Bandyopadhyay, R. Khattar, T. P. Fehlner, *Inorg. Chem.* **1989**, *28*, 4434–4436.
[103] A. K. Bandyopadhyay, R. Khattar, J. Puga, T. P. Feglner, A. L. Rheingold, *Inorg. Chem.* **1992**, *31*, 465–472.
[104] A. D. Hattersley, C. E. Housecroft, A. L. Rheingold, *J. Clust. Sci.* **1997**, *8*, 329–348.
[105] A. D. Hattersley, C. E. Housecroft, A. L. Rheingold, *J. Chem. Soc. Dalton Trans.* **1996**, 603–610.
[106] B. Berti, C. Cesari, C. Femoni, T. Funaioli, M. C. Iapalucci, S. Zacchini, *Dalton Trans.* **2020**, *49*, 5513–5522.
[107] C. Cesari, T. Funaioli, B. Berti, C. Femoni, M. C. Iapalucci, F. M. Vivaldi, S. Zacchini, *Inorg. Chem.* **2021**, *60*, 16713–16725.
[108] S. Hossain, Y. Niihori, L. V. Nair, B. Kumar, W. Kurashige, Y. Negishi, *Acc. Chem. Res.* **2018**, *51*, 3114–3124.
[109] S. Wang, Q. Li, X. Kang, M. Zhu, *Acc. Chem. Res.* **2018**, *51*, 2784–2792.
[110] C. Femoni, M. C. Iapalucci, G. Longoni, S. Zacchini, *Eur. J. Inorg. Chem.* **2009**, *2009*, 2487–2495.
[111] A. Ceriotti, R. Della Pergola, G. Longoni, M. Manassero, M. Sansoni, *J. Chem. Soc. Dalton Trans.* **1984**, 1181–1186.

[112] A. Ceriotti, G. Longoni, M. Manassero, M. Sansoni, R. Della Pergola, B. T. Heaton, D. O. Smith, *J. Chem. Soc. Chem. Commun.* **1982**, 886–887.
[113] E. Brivio, A. Ceriotti, R. Della Pergola, L. Garlaschelli, F. Demartin, M. Manassero, M. Sansoni, P. Zanello, F. Laschi, B. T. Heaton, *J. Chem. Soc. Dalton Trans.* **1994**, 3237–3242.
[114] C. Cesari, B. Berti, M. Bortoluzzi, C. Femoni, M. C. Iapalucci, S. Zacchini, *Inorg. Chem.* **2021**, *60*, 8811–8825.
[115] A. Ceriotti, F. Demartin, G. Longoni, M. Manassero, M. Marchionna, G. Piva, M. Sansoni, *Angew. Chem. Int. Ed.* **1985**, *24*, 697–698.
[116] N. de Silva, L. F. Dahl, *Inorg. Chem.* **2006**, *45*, 8814–8816.
[117] C. Femoni, M. C. Iapalucci, G. Longoni, P. H. Svensson, P. Zanello, F. Fabrizi de Biani, *Chem. Eur. J.* **2004**, *10*, 2318–2326.
[118] C. Femoni, M. C. Iapalucci, G. Longoni, P. H. Svensson, *Chem. Commun.* **2004**, 2274–2275.
[119] C. Cesari, B. Berti, M. Bortoluzzi, C. Femoni, T. Funaioli, F. M. Vivaldi, M. C. Iapalucci, S. Zacchini, *Dalton Trans.* **2023**, *52*, 3623–3642.
[120] B. Berti, M. Bortoluzzi, C. Cesari, C. Femoni, M. C. Iapalucci, L. Soleri, S. Zacchini, *Inorg. Chem.* **2020**, *59*, 15936–15952.
[121] J. Fu, M. Morshedi, G. J. Moxey, A. Barlow, M. P. Cifuentes, M. G. Humphrey, *Chem. Eur. J.* **2016**, *22*, 5128–5132.
[122] S. Banerjee, M. K. Karunananda, S. Bagherzadeh, U. Jayarathne, S. R. Parmelee, G. W. Waldhart, N. P. Mankad, *Inorg. Chem.* **2014**, *53*, 11307–11315.
[123] B. Berti, M. Bortoluzzi, C. Cesari, C. Femoni, M. C. Iapalucci, R. Mazzoni, F. Vacca, S. Zacchini, *Inorg. Chem.* **2019**, *58*, 2911–2915.
[124] A. Cervellino, A. Maspero, N. Masciocchi, A. Guaglairdi, *Growth Des.* **2012**, *12*, 3631–3637.
[125] P. Klüfers, *Angew. Chem. Int. Ed.* **1984**, *23*, 307–308.
[126] P. Klüfers, *Angew. Chem. Int. Ed.* **1985**, *24*, 70–71.
[127] C. Femoni, R. Della Pergola, M. C. Iapalucci, F. Kaswalder, M. Riccò, S. Zacchini, *Dalton Trans.* **2009**, 1509–1511.
[128] A. F. Abdel-Magied, Y. Theibich, A. K. Singh, A. Rahaman, I. Doverbratt, A. K. Raha, M. Haukka, M. G. Richmond, E. Nordlander, *Dalton Trans.* **2020**, *49*, 4244–4256.
[129] P. Homanen, R. Persson, M. Haujja, T. A. Pakkanen, E. Nordlander, *Organometallics* **2000**, *19*, 5568–5574.
[130] J. Dong, Z.-H. Gao, Q.-F. Zhang, L.-S. Wang, *Angew. Chem. Int. Ed.* **2021**, *60*, 2424–2430.
[131] T.-H. Chiu, J.-H. Liao, F. Gam, Y.-Y. Wu, X. Wang, S. Kahlal, J.-Y. Saillard, C. W. Liu, *J. Am, Chem. Soc.* **2022**, *144*, 10599–10607.
[132] S.-F. Yuan, Z.-J. Guan, Q.-M. Wang, *J. Am. Chem. Soc.* **2022**, *144*, 11405–11412.

Manuscript received: April 17, 2024
Revised manuscript received: July 8, 2024
Accepted manuscript online: September 18, 2024
Version of record online: October 30, 2024